Multispecific DARPin® therapeutics demonstrate very high potency against SARS-CoV-2 variants *in vitro*

Sylvia Rothenberger[1,2,*], Marcel Walser[3,*], Francesca Malvezzi[3], Jennifer Mayor[1,2], Sarah Ryter[1], Hector Moreno[2], Nicole Liechti[1], Silvan Hälg[4], Andreas Bosshart[3], Chloe Iss[3], Valérie Calabro[3], Andreas Cornelius[3], Tanja Hospodarsch[3], Alexandra Neculcea[3], Thamar Looser[3], Rachel Herrup[5], Sabrina Lusvarghi[5], Sabari Nath Neerukonda[5], Russell Vassell[5], Wei Wang[5], Susanne Mangold[3], Christian Reichen[3], Filip Radom[3], Keith M. Dawson[3], Seth Lewis[3], Daniel Steiner[3], Carol D. Weiss[5], Patrick Amstutz[3], Olivier Engler[1,**], Michael T. Stumpp[3,6,**]

* These first authors contributed equally to this work

** These senior authors contributed equally to this work

[1]Spiez Laboratory, Austrasse, 3700 Spiez, Switzerland

[2]Institute of Microbiology, University Hospital Center and University of Lausanne, Rue du Bugnon 48, 1011 Lausanne, Switzerland

[3]Molecular Partners AG, Wagistrasse 14, 8952 Zurich-Schlieren, Switzerland

[4]Swiss Tropical and Public Health Institute, Department Epidemiology and Public Health, Basel, Switzerland. University of Basel, Basel, Switzerland.

[5]Laboratory of Immunoregulation, Division of Viral Products, Center for Biologics Evaluation and Research, U.S. Food and Drug Administration, Silver Spring, Maryland, USA

[6]To whom correspondence should be addressed:

Michael T. Stumpp

+41 44 755 77 00

info@molecularpartners.com

Keywords: SARS-CoV-2, COVID-19, corona virus, mutations, ensovibep, emerging variants, antiviral therapy, viral passaging, DARPin® drug, ankyrin repeat protein, multispecific, K417N, K417T, L452R E484K, N501Y, B.1.1.7, B.1.351, P.1, B.1.429, B.1.526, B.1.617, B.1.618, MP0420, MP0423

DARPin® is a registered trademark owned by Molecular Partners AG

Abstract

The SARS-CoV-2 virus responsible for the COVID-19 pandemic has so far infected more than 160 million people globally, and continues to undergo genomic evolution. Emerging SARS-CoV-2 variants show increased infectivity and may lead to resistance against immune responses of previously immunized individuals or existing therapeutics, especially antibody-based therapies.

Several monoclonal antibody therapeutics authorized for emergency use or in development have been shown to lose potency against some SARS-CoV-2 variants. Cocktails of two different monoclonal antibodies constitute a promising approach to protect against novel emerging variants as long as both antibodies are potent, but come with increased development complexity and therefore cost. As an alternative, we developed two multispecific DARPin® therapeutics, each combining three independent DARPin® domains binding the SARS-CoV-2 spike protein in one molecule, to potently neutralize the virus and overcome virus escape.

Here, we show in a panel of *in vitro* studies that the multispecific DARPin® therapeutic design incorporated in our clinical candidate ensovibep (MP0420), achieved high neutralization potencies against the circulating SARS-CoV-2 variants B.1.1.7 (UK variant), B.1.351 (South African variant), P.1 (Brazilian variant), B.1.429 (South Californian variant), B.1.526 (New York variant), R.1 (Japanese variant), A.23.1 (Ugandan variant), and B.1.617 (Indian variant), and there is strong evidence that ensovibep also potently neutralizes the Indian variant B.1.618 based on the analysis of the key point mutations in the spike protein of this variant. Additionally, viral passaging experiments show potent protection by ensovibep and MP0423 against development of escape mutations. Finally, we demonstrate that the cooperative binding of the individual modules in a multispecific DARPin® antiviral is key for potent virus inhibition and protection from escape variants. These results, combined with the relatively small size and high production yields of DARPin® molecules, suggest that ensovibep is a highly valuable alternative to monoclonal antibody cocktails for global supply and demonstrate the strength of the DARPin® platform for achieving potent and lasting virus inhibition for SARS-CoV-2 and possibly other viruses.

Introduction

As the COVID-19 pandemic progresses, new circulating variants of SARS-CoV-2 have been described that show resistance against the immune response of previously immunized individuals[1,2] or available therapeutics[3,4]. In many regions around the globe, governments are implementing lock-down measures to contain rapidly spreading SARS-CoV-2 spike variants associated with increased transmissibility[5]. Variants first isolated in the UK (B.1.1.7 lineage), South Africa (B.1.351)[6], Brazil (P.1)[2], South California (B.1.429), New York, (B.1.526), Japan (R.1), Uganda (A.23.1) or the newest emerging variants in India (lineages B.1.617 and B.1.618) share mutations on the spike protein, which have evolved independently. Amongst those, mutations K417E/N/T, L452R, E484K and N501Y are of major concern, as these residues are associated with an enforced receptor binding[7], and thus increased transmissibility and/or immune escape of the virus[3,8-11].

Other mutations confer resistance against monoclonal antibody therapeutics, including N439K, where independent lineages were originally detected in Scotland, subsequently in Romania and then spread in many countries such as the USA[3]. Further amino acid changes, which may reduce therapeutic options are Y453F, which evolved in Danish mink farms[12], and less common mutations, such as G446V, G476S, T478I, P479S, V483A, F486V, F490S and Q493K, originally described by Baum et al.[13]. Additional mutations which occur globally at high frequencies such as A222V, S477N, D614G and Q675H[14-16] are considered less of a concern to date.

To circumvent the loss of potency of single monoclonal neutralizing antibodies, antibody cocktails were generated, providing a higher resistance against escape mutations[13,17,18]. However, this strategy is associated with increased manufacturing costs and limited global supply capacities[19].

We have applied our DARPin® platform that allows fast generation and cost-effective production of multispecific therapeutics to generate anti-SARS-CoV-2 multispecific DARPin® antivirals, with very high neutralizing potencies, which were described previously[20]. In brief, DARPin® molecules are structurally completely different from antibodies and consist of a single chain of linked DARPin® domains; in this case the molecules have two human serum albumin binding domains for systemic half-life extension and three spike protein binding domains at the C-terminus. The relatively small size of these multispecific DARPin® antivirals, in the range of 75-85 kDa, in conjunction with the high thermal stability, solubility and very high production yields make these molecules an attractive therapeutic alternative to antibody cocktails.

Two of these DARPin® antivirals, ensovibep and MP0423, are currently in clinical and pre-clinical development. The viral inhibition mode of ensovibep is based on three distinct DARPin® domains targeting the Receptor Binding Domain (RBD) while MP0423 has three DARPin® domains directed to three different domains of the spike protein: the RBD, the N Terminal Domain (NTD) and the S2 domain.

90 Here, we demonstrate that our clinical candidate, ensovibep, confers full protection against a panel of
91 relevant spike mutations as well as eight SARS-CoV-2 variants recently identified around the globe
92 (B.1.1.7, B.1.351[6], P.1[2], B.1.429, B.1.526, R.1, A.23.1, B.1.617) or the key mutations of the emerging
93 variant in India, B.1.618. In addition, we show in a viral passaging experiment that the multispecific
94 DARPin® antivirals' protection against development of viral escape mutants is comparable to that of
95 the best characterized and efficacious monoclonal antibody cocktail to date[13,18,21]. These data confirm
96 that the tripartite design is successful against emerging mutations and strongly validates the further
97 development of ensovibep as a potent therapeutic against COVID-19.

98 # Results

99

100 *Ensovibep is highly potent against globally identified SARS-CoV-2 variants as well as the most frequent*
101 *spike protein point mutations*

102 The spike protein of SARS-CoV-2 mediates cell entry through binding to the human ACE2 receptor.
103 SARS-CoV-2 is also capable of infecting non-primate hosts, such as felines and minks[22]. The promiscuity
104 of a multi-host life style is often an indicator of early, still sub-optimal adaptation of the virus to its new
105 host. This suggests inherent dynamic plasticity and potential for further human adaptation. The
106 receptor-binding domain (RBD) in the spike protein forms the interface with human ACE2. Site
107 mutagenesis scanning and structure analysis revealed critical residues for this interaction, i.e. L455,
108 F456, A475, F486, F490 and Q493[8,23]. Notably, single amino acid substitutions N439R, L452K, T470N,
109 E484P, Q498Y and N501T have been shown to increase the affinity for human ACE2[8]. Consistent with
110 these experimental findings, mutations K417N, K417T, L452R, E484K, and N501Y appeared in rapidly
111 spreading SARS-CoV-2 spike variants in association with facilitated receptor binding and increased
112 transmissibility[3,9,24]. The RBD domain is also immunogenic, and among others residues, K417, L452,
113 K444, E484, and F486 have been shown to be critical for the binding of neutralizing antibodies[17].

114 In the present study we analyzed the impact of selected critical variants and mutated residues on the
115 neutralization capacity of ensovibep and MP0423 (Figure 1). To assess the potency of the monospecific
116 and multispecific DARPin® molecules, we used VSV-based as well as lentivirus-based pseudoviruses
117 carrying the SARS-CoV-2 wild-type or mutant spike protein at their surface or variants of authentic
118 SARS-CoV-2 for lineages B.1.1.7, B.1.351 and P.1. The pseudoviruses as well as the authentic SARS-CoV-
119 2 variants were used in neutralization tests with multispecific DARPin® molecules ensovibep and
120 MP0423 or control neutralizing antibodies REGN10933 and REGN10987. A summary of the calculated
121 IC_{50} values are reported in Table 1a, Table 1b and Table 1c.

122 The results show that ensovibep can neutralize variants of the lineage B.1.1.7 (69-70 del, del145, E484K,
123 N501Y, A570D, D614G, P681H, T716I, S982A, D1118H), lineage B.1.351 (D80A, D215G, Del242-244,
124 R246I, K417N, E484K, N501Y, D614G, A701V), lineage P.1 (L18F, T20N, P26S, D138Y, R190S, K417T,
125 E484K, N501Y, D614G, H655Y, T1027I, V1176F), lineage B.1.429 (S13I, P26S, W152C, L452R, D614G),
126 lineage B.1.526 (L5F, T95I, D253G, E484K, D614G, A701V), lineage B.1.617, recently originating from
127 India (G142D, E154K, V382L, L452R, E484Q, D614G, P681R, Q1071H, D1153Y) and the most critical
128 point mutations of the Indian variant B.1.618 (del 145, L452R, E484Q, E484K, D614G) as efficiently as
129 the wild-type virus with IC_{50} values in the low single-digit ng/mL range. While MP0423 remained highly
130 potent against the B.1.351 (Δ5) and B.1.526 (Δ6) variant, it lost some potency to the double-digit or low
131 triple-digit ng/mL range for B.1.1.7(Δ10), B.1.351(Δ9), P.1 (Δ12), B.1.429 (Δ5). The observed potency

132 drop is thought to be caused by mutations in the S2 domain alone or in combination with the NTD
133 mutations, as a reduction in potency for MP0423 was observed for point mutations D80A, R246I, P681H
134 and deletions 145 or 244-246. The structural determinants responsible for this potency drop are
135 currently under investigation
136 Notably, ensovibep protected well against all individual mutations tested, with the only exception of
137 the mutation F486V, which affects all three monovalent DARPin® RBD binders incorporated in
138 ensovibep.
139 As F486 is a critical residue for the interaction between RBD and human ACE2, selective pressure on
140 the virus favors its conservation, thus maintaining an important anchoring element for the binding of
141 ensovibep. A major impact of this mutation on ensovibep is not surprising, as previous structural
142 analysis identified F486 as a core interacting residue for the three related but different RBD binders[20].
143 Consequently, the mutation F486V destabilizes the binding of the entire tri-specific ensovibep molecule
144 to the spike protein.
145 Taken together, our analysis confirms that ensovibep is highly potent against spike proteins carrying
146 the most frequently observed mutations as well as mutations known to impact the binding of
147 neutralizing antibodies, as expected from the multispecific design.
148
149 *Passaging of SARS-CoV-2 under therapeutic pressure of DARPin® antivirals and monoclonal antibodies*
150 Previous studies have shown that viral escape mutants may rapidly appear under selective pressure of
151 a therapy[1,17]. We used a viral passaging model adapted from Baum et al.[13] to estimate the risk of viral
152 escape from therapeutic pressure of ensovibep, MP0423 and of a cocktail of the two Regeneron
153 monoclonal antibodies REGN10933 & REGN10987, in comparison to the monovalent DARPin® binder
154 RBD-2 and to the monoclonal antibodies S309, REGN10933 and REGN10987 applied as single
155 molecules.
156 1.5 x 10^6 pfu of a French SARS-CoV-2 isolate (with the following differences to the Wuhan wild-type:
157 V367F; E990A) were serially passaged in the presence of increasing concentrations of DARPin®
158 molecules and antibodies (Figure 2A, Figure 2B). Resistant escape variants were further selected by
159 passaging the supernatant of cultures showing significant virus-induced cytopathic effect (CPE) under
160 the selection pressure of the highest therapeutic concentration onto fresh cells while maintaining the
161 selective pressure of increasing concentrations of therapeutic antivirals. After the first incubation cycle
162 of four days (passage 1) the monovalent DARPin® binder RBD-2 and the multispecific DARPin® antivirals,
163 as well as the antibody antivirals REGN10933 and the antibody cocktail (REGN10933 & REGN10987)
164 conferred protection at the same concentration of 0.4 µg/mL. The monoclonal antibody S309 was less
165 efficient, requiring a higher concentration (10 µg/mL) for protection and the monoclonal antibody

166 REGN10987 was not protective up to the highest concentration tested of 50 µg/mL. Under continuous
167 selective pressure through passage 2 to 4, the monovalent DARPin® binder RBD-2, and the individual
168 monoclonal antibodies S309 and REGN10933 lost the capacity to protect cells, which manifested in
169 complete CPE up to the highest concentration tested. In contrast, ensovibep and MP0423, as single
170 molecules or in combination, and the cocktail of two monoclonal antibodies remained effective and
171 protected cells from CPE throughout the 4 passages.
172 While the application of ensovibep and MP0423 as single agents required higher concentrations,
173 respectively 2 µg/mL and 10 µg/mL, after 4 passages, the combination of the two DARPin® antivirals
174 retained effectiveness at a low concentration of 0.08 µg/mL. The mixture of the two monoclonal
175 antibodies, REGN10933 & REGN10987, prevented the selection of escape mutants at a concentration
176 of 0.4 µg/mL after passage 4.
177 To identify putative escape mutations in the spike protein, RNA was extracted and sequenced from
178 supernatant of wells with the greatest selective pressure showing a significant cytopathic effect (Suppl.
179 Fig. 4). Amongst mutations near the spike protein cleavage site (H655Y, N679_R685del, R682W,
180 R682Q), which might likely be related to adaptations to the used cell system[36, 37], a potential escape
181 mutation, F486L, was found for the monovalent RBD binder (RBD-2), which is incorporated in
182 ensovibep. In addition, a potential deletion at position F140 was identified, which might reduce the
183 potency of MP0423.

184 # Discussion

185

186 Novel emerging variants of the virus are an ever-present threat, as they may escape the antibodies
187 generated during immunization or developed as therapeutics.
188 Here, we showed that our multispecific DARPin® clinical candidate ensovibep gives high levels of
189 protection against the currently most frequently reported SARS-CoV-2 mutations as well as recently
190 identified variants. Neutralization tests using VSV-based as well as lentivirus-based pseudoviruses
191 carrying SARS-CoV-2 spike variants as well as infectious SARS-CoV-2 showed inhibitory potencies for
192 ensovibep that were comparable to that for the corresponding wild type. While MP0423 also remained
193 active against some tested variants, a partial potency decrease was observed for most of the tested
194 variants of concern. Of note, this lowered potency is still in an active potency range described by many
195 monoclonal antibodies.
196 In the present study we investigated a panel of single mutations, shown to be of concern because they
197 may be associated with increased transmissibility, or have an impact on disease severity, or affect
198 neutralization by some polyclonal or monoclonal antibodies[13,25,26]. Among all mutations tested, only
199 F486V caused a strong decrease in potency for ensovibep, when compared to the wild-type. In
200 accordance, deep sequencing of the viral passaging supernatant for the monovalent RBD binder (RBD-
201 2, incorporated in ensovibep) also revealed F486L as a potential mutation for the virus to escape the
202 treatment (Suppl. Fig. 4). These findings are in line with our previous structural analysis[20] showing that
203 F486 is one of the key binding residues for the interaction with ensovibep and the RBD. Most
204 importantly, F486 is a critical residue for the virus itself, allowing an efficient binding to the ACE2
205 receptor and thus cell infection. Therefore, mutations of the phenylalanine at position 486 will decrease
206 the affinity between the RBD and human ACE2 receptor and lower the infectivity of the virus[10,27-29]. To
207 date, mutations at position F486 are not present at high frequency in circulating SARS-CoV-2 strain.
208 Interestingly, the single point mutation F486V does not affect the neutralizing capacity of MP0423,
209 despite the fact that it contains a RBD binder for which F486 is a critical residue. These findings,
210 summarized in Suppl. Fig.2, highlight the strength of the tri-epitopic DARPin design. In this approach, a
211 loss of binding of one DARPin domain might be compensated by the binding via the two remaining
212 DARPin domains of the molecule.
213 In the same line, some mutations, that are not predicted as key interaction residues for the three
214 distinct RBD binders of ensovibep (e.g. E484K or Q493K), led to a reduction of the potency in one or
215 several of the RBD binders, while the trispecific ensovibep molecule maintained the full neutralization
216 capacity. This demonstrates that a tri-specific DARPin® design with cooperative binding permits high
217 potency inhibition, even in the case one DARPin® domain is losing neutralization capacity when the

218 domain is evaluated separately. This cooperativity is an exclusive feature of a trispecific approach,
219 highlighting a key advantage of the multispecific DARPin® design over cocktails of antibodies.
220 The high level of protection against viral escape mutations by ensovibep and MP0423 was further
221 demonstrated in a viral passaging experiment: the single monoclonal antibodies and the monovalent-
222 DARPin® RBD-2 binder were rapidly overcome by escape mutants, whereas both multispecific DARPin®
223 antivirals, individually or in combination, maintained potency up to passage 4, to an extent comparable
224 to one of the best monoclonal antibody cocktails with emergency use authorization (EUA) status in the
225 USA.
226 The high level of neutralization of multispecific DARPin® antivirals against mutations and variants
227 evaluated in this study encourages the characterizations of future upcoming mutations and will remain
228 an ongoing topic for COVID-19 diagnostics, therapeutics and vaccines.

Acknowledgements

The authors thank Dr. Gert Zimmer for the gift of the recombinant VSV (Institute of Virology and Immunology (IVI), CH-3147 Mittelhäusern, Switzerland, Department of Infectious Diseases and Pathobiology, Vetsuisse Faculty, University of Bern, CH-3012 Bern, Switzerland).

The expression plasmid for the SARS-CoV-2 spike protein was kindly provided by Dr. Giulia Torriani and Dr. Isabella Eckerle (Department of Medicine, University of Geneva, Switzerland).

SR & JM were supported by Swiss Federal Office for Civil Protection (Grants Nr. 353008564/Stm, 353008218/Stm, and 353008560/Stm to Olivier Engler and Stefan Kunz).

We would like to thank for the supply of the two 2019-nCoV strains: i) 2019-nCoV/IDF0372/2020 provided by the National Reference Centre for Respiratory Viruses hosted by Institute Pasteur (Paris, France) and headed by Dr. Sylvie van der Werf.

We would like to thank for the VeroE6/TMPRSS2 cells obtained by the Centre for AIDS Reagents (National Institute for Biological Standards and Control, Herts, UK).

Support for this research was provided by ACTIV, a public-private partnership, to develop a coordinated research strategy to speed the most promising COVID-19 vaccines and treatments.

Funding

All studies were funded by Molecular Partners AG, Switzerland, and NIH/ACTIV, US.

Author contributions

S.Ro.; M.W.; F.M.; J.M.; S.Ry.; A.B.; V.C.; P.A.; M.S; O.E.: conceptualized and designed experiments; S.Ro.; J.M.; S.Ry; H.M; N.L.; S.H.; A.B.; C.I.; A.C.; T.H.; A.N.; R.H.; S.Lu.; R.V.; S.N.N.; W.W.; T.L.; S.M.; C.D.W.: performed laboratory experiments; F.M.; C.R.; F.R.: performed computational work; S.Ro.; M.W.; F.M.; J.M.; S.Ry.; H.M.; N.L.; S.H.; A.B.; C.I.; A.C.; C.R.; F.R.; K.D.; S.Le.; P.A.; M.S.; O.E.: drafted the manuscript; S.Le.; D.S; P.A.; M.S.: acquired funding; All authors reviewed the manuscript.

Competing interests: Molecular Partners authors own performance share units and/or stock of the company.

Figures

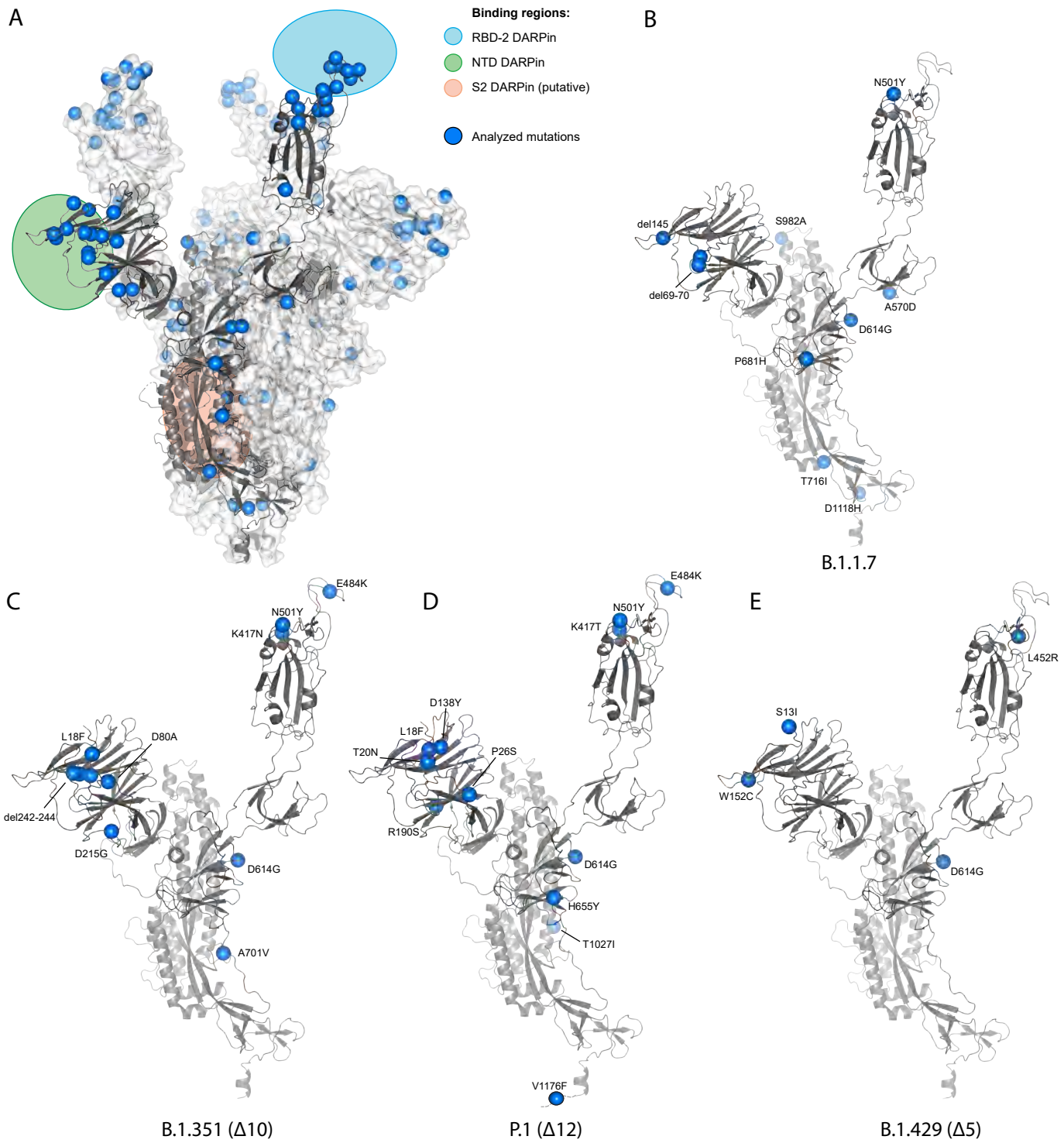

Figure 1: Structural visualization of critical mutations of the SARS-CoV-2 spike protein evaluated in this study. A) Representation of the full trimeric SARS-CoV-2 spike protein with all residues analyzed in the study visualized as blue spheres. Binding regions for the individual DARPin® domains incorporated in ensovibep and MP0423 are colored in blue (RBD), green (NTD) and orange (S2); B-E) Monomeric spike protein structures representing B) the variant first identified in the UK B.1.1.7 (del69-70, del145, N501Y, A470D, D614G, P681H, T716I, S982A, D1118H); C) the variant first identified in South Africa B.1.351 (L18F, D80A, D215G, del242-244, R246I, K417N, E484K, N501Y, D614G, A701V); D) the variant first identified in Brazil P.1 (L18F, T20N, P26S, D138Y, R190S, K417T, E484K, N501Y, D614G, H655Y, T1027I, V1176F); E) the variant first identified in California, US (S13I, W152C, L452R, D614G). The PDB file 6xcn was used for generating the figures with PyMol version 2.1.1 (Schrödinger, LLC). In order to visualize all mutations, flexible loops, and regions of the NTD domain missing in the structure, were modelled with MODELLER included in the BIOVIA Discovery Studio software using the PDB file 6zge as template for the NTD domain (BIOVIA, Dassault Systèmes, BIOVIA Discovery Studio 2021).

A

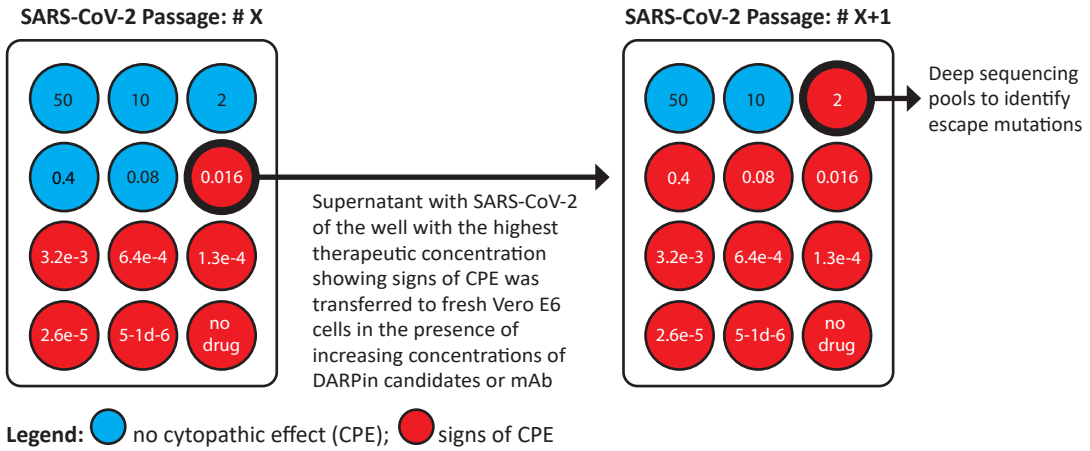

B

Passage #1	DARPin or Antibody Concentrations [µg/mL]						
Constructs	50	10	2	0.4	0.08	0.02	no drug
DARPin Candidates	Cytopathic Effect [%]						
RBD - 2	0%	0%	0%	5%	≥90%	≥90%	≥90%
ensovibep	0%	0%	0%	0%	≥90%	≥90%	≥90%
MP0423	0%	0%	0%	0%	≥90%	≥90%	≥90%
MP0420 & MP0423	0%	0%	0%	0%	≥90%	≥90%	≥90%
Antibody Candidates	Cytopathic Effect [%]						
S309	0%	0%	60%	≥90%	≥90%	≥90%	≥90%
REGN10933	0%	0%	0%	5%	80%	≥90%	≥90%
REGN10987	80%	≥90%	≥90%	≥90%	≥90%	≥90%	≥90%
REGN10933 & REGN10987	0%	0%	0%	0%	≥90%	≥90%	≥90%
IgG Negative Control	≥90%	≥90%	≥90%	≥90%	≥90%	≥90%	≥90%

Passage #2	DARPin or Antibody Concentrations [µg/mL]						
Constructs	50	10	2	0.4	0.08	0.02	no drug
DARPin Candidates	Cytopathic Effect [%]						
RBD - 2	0%	60%	≥90%	≥90%	≥90%	≥90%	≥90%
ensovibep	0%	0%	0%	0%	0%	50%	≥90%
MP0423	0%	0%	0%	0%	0%	≥90%	≥90%
MP0420 & MP0423	0%	0%	0%	0%	0%	≥90%	≥90%
Antibodies Candidates	Cytopathic Effect [%]						
S309	≥90%	≥90%	≥90%	≥90%	≥90%	≥90%	≥90%
REGN10933	0%	0%	80%	≥90%	≥90%	≥90%	≥90%
REGN10987	≥90%	≥90%	≥90%	≥90%	≥90%	≥90%	≥90%
REGN10933 & REGN10987	0%	0%	0%	0%	0%	≥90%	≥90%
IgG Negative Control	≥90%	≥90%	≥90%	≥90%	≥90%	≥90%	≥90%

Passage #3	DARPin or Antibody Concentrations [µg/mL]						
Constructs	50	10	2	0.4	0.08	0.02	no drug
DARPin Candidates	Cytopathic Effect [%]						
RBD - 2	≥90%	≥90%	≥90%	≥90%	≥90%	≥90%	≥90%
ensovibep	0%	0%	0%	0%	≥90%	≥90%	≥90%
MP0423	0%	0%	0%	40%	≥90%	≥90%	≥90%
MP0420 & MP0423	0%	0%	0%	0%	≥90%	≥90%	≥90%
Antibodies Candidates	Cytopathic Effect [%]						
S309	≥90%	≥90%	≥90%	≥90%	≥90%	≥90%	≥90%
REGN10933	0%	0%	5%	≥90%	≥90%	≥90%	≥90%
REGN10987	≥90%	≥90%	≥90%	≥90%	≥90%	≥90%	≥90%
REGN10933 & REGN10987	0%	0%	0%	0%	≥90%	≥90%	≥90%
IgG Negative Control	≥90%	≥90%	≥90%	≥90%	≥90%	≥90%	≥90%

Passage #4	DARPin or Antibody Concentrations [µg/mL]						
Constructs	50	10	2	0.4	0.08	0.02	no drug
DARPin Candidates	Cytopathic Effect [%]						
RBD - 2	n.d.	n.d.	n.d.	n.d.	n.d.	n.d.	n.d.
ensovibep	0%	0%	0%	40%	≥90%	≥90%	≥90%
MP0423	0%	0%	≥90%	≥90%	≥90%	≥90%	≥90%
MP0420 & MP0423	0%	0%	0%	0%	5%	≥90%	≥90%
Antibodies Candidates	Cytopathic Effect [%]						
S309	n.d.	n.d.	n.d.	n.d.	n.d.	n.d.	n.d.
REGN10933	≥90%	≥90%	≥90%	≥90%	≥90%	≥90%	≥90%
REGN10987	n.d.	n.d.	n.d.	n.d.	n.d.	n.d.	n.d.
REGN10933 & REGN10987	0%	0%	0%	0%	≥90%	≥90%	≥90%
IgG Negative Control	n.d.	n.d.	n.d.	n.d.	n.d.	n.d.	n.d.

Figure 2: Ensovibep and MP0423 protect from viral escape mutants*:* A) Schematic representation of the procedure: French SARS-CoV-2 isolate from early 2020 (1.5 x10^6 pfu) was incubated in presence of increasing concentrations of DARPin® or antibody for 4 days on Vero E6 cells and virus-induced cytopathic effects (CPE) were determined by microscopy. For each DARPin® and antibody condition, cultures showing significant cytopathic effect (≥20%) under the greatest selective pressure were selected and virus-containing supernatant collected to start a new culture passage on Vero E6 cells, again under increasing concentrations of the corresponding DARPin® or monoclonal antibody condition. Passaging of virus containing supernatant was continued in the same manner for a total of 4 passages. B) Tabular representation of the cytopathic effects induced by SARS-CoV-2 cultured in presence of increasing concentrations of mono-valent DARPin® binder RBD-2, multi-specific DARPin® antivirals ensovibep and MP0423 or a cocktail of ensovibep and MP0423 and the antibody antivirals S309, REGN10933 and REGN10987 or a cocktail of REGN10933 and REGN10987 through passage 1 to 4. A cytopathic effect (CPE) judged by microscopy to be less than 20% is colored in blue and a CPE estimated ≥20% is colored in red. Indicated with a dark border are the culture supernatants chosen for further passaging under selective pressure and for deep sequencing (data in process).

257 # Tables

258 **Table 1a: Summary of the neutralizing efficacy of multispecific DARPin® candidates and monoclonal**
259 **antibodies against VSV or Lentivirus SARS-CoV-2 pseudoviruses carrying spike variants as well as authentic**
260 **SARS-CoV-2 variants.** Neutralization tests for multispecific DARPin® candidates, ensovibep and MP0423
261 and two neutralizing antibodies, REGN10933 and REGN10987, were performed and IC_{50} (ng/mL) values
262 are shown for each experimental condition.

Lineage (Origin)	Variants and Point Mutations analyzed	Assay Type	VSV or Lentivirus Pseudotype Neutralizaiton Assay IC_{50} [ng/mL]			
			MP0420	MP0423	REGN10933	REGN10987
Reference	Wuhan wild type	VSV	1.0	3.1	3.9	6.0
	D614G	Lentivirus	1.1	3.0	n.a.	n.a.
B.1.1.7 / United Kingdom	69-70 del, del145, N501Y, A570D, D614G, P681H, T716I, S982A, D1118H	VSV	1.7	70	2.4	3.5
	69-70 del, del145, E484K, N501Y, A570D, D614G, P681H, T716I, S982A, D1118H	VSV	3.2	77	30	1.6
	69-70 del, del145, N501Y, A570D, D614G, P681H, T716I, S982A, D1118H	Lentivirus	0.9	58	n.a.	n.a.
	69-70 del, del145, S494P, N501Y, A570D, D614G, P681H, T716I, S982A, D1118H	Lentivirus	0.8	50	n.a.	n.a.
	del69-70	VSV	1.9	5.0	4.1	4.1
	del145	VSV	2.1	9.7	1.9	3.9
	N501Y	VSV	0.6	1.7	2.1	1.0
	A570D	VSV	1.2	2.4	0.2	1.3
	D614G	VSV	2.4	2.8	n.a.	n.a.
	P681H	VSV	1.5	10.1	1.3	3.5
	T716I	VSV	0.6	0.3	0.7	3.2
	S982A	VSV	2.0	0.9	1.0	10.0
	D1118H	VSV	2.6	0.6	2.0	2.3
B.1.351 / South Africa	D80A, D215G, E484K, N501Y, A701V	VSV	5.5	2.4	19.4	2.9
	L18F, D80A, D215G, Del242-244, R246I, K417N, E484K, N501Y, D614G, A701V	VSV	5.0	31	15.4	1.3
	L18F, D80A, D215G, Del242-244, K417N, E484K, N501Y, D614G, A701V	Lentivirus	1.2	116	n.a.	n.a.
	L18F	VSV	3.5	1.9	3.5	3.0
	D80A	VSV	3.6	17.1	n.a.	n.a.
	D215G	VSV	4.6	2.6	n.a.	n.a.
	del242-244	VSV	2.0	130	1.8	2.0
	R246I	VSV	1.3	34	2.3	3.0
	K417N	VSV	0.6	0.7	n.a.	n.a.
	E484K	VSV	2.7	1.8	17.0	5.8
	N501Y	VSV	0.6	1.7	2.1	0.9
	D614G	VSV	2.4	2.8	n.a.	n.a.
	A701V	VSV	1.1	1.0	n.a.	n.a.

P.1 / Brazil	L18F, T20N, P26S, D138Y, R190S, K417T, E484K, N501Y, D614G, H655Y, T1027I	VSV	1.2	8.3	32.4	1.0
	L18F, T20N, P26S, D138Y, R190S, K417T, E484K, N501Y, D614G, H655Y, T1027I, V1176F	Lentivirus	0.7	34.0	n.a.	n.a.
	L18F	VSV	3.5	1.9	3.5	3.0
	T20N	VSV	4.6	7.6	n.a.	n.a.
	P26S	VSV	1.8	3.4	n.a.	n.a.
	D138Y	VSV	2.2	5.2	n.a.	n.a.
	R190S	VSV	1.7	2.2	n.a.	n.a.
	K417T	VSV	0.5	0.6	n.a.	n.a.
	E484K	VSV	2.7	1.8	17.0	5.8
	N501Y	VSV	0.6	1.7	2.1	0.9
	D614G	VSV	2.4	2.8	n.a.	n.a.
	H655Y	VSV	2.4	1.4	n.a.	n.a.
	T1027I	VSV	3.3	2.8	n.a.	n.a.
B.1.429 / California (US)	S13I, W152C, L452R, D614G	Lentivirus	0.9	174	n.a.	n.a.
	S13I, P26S, W152C, L452R, D614G	Lentivirus	0.5	124	n.a.	n.a.
	S13I		n.a.	n.a.	n.a.	n.a.
	P26S	VSV	1.8	3.4	n.a.	n.a.
	W152C		n.a.	n.a.	n.a.	n.a.
	L452R	Lentivirus	0.5	1.4	n.a.	n.a.
	D614G	VSV	2.4	2.8	n.a.	n.a.
B.1.526 / New York (US)	L5F, T95I, D253G, E484K, D614G, A701V	Lentivirus	3.0	3.8	n.a.	n.a.
	L5F	Lentivirus	1.1	2.2	n.a.	n.a.
	T95I	Lentivirus	0.9	2.2	n.a.	n.a.
	D253G	Lentivirus	1.0	3.1	n.a.	n.a.
	E484K	VSV	2.7	1.8	17.0	5.8
	D614G	VSV	2.4	2.8	n.a.	n.a.
	A701V	VSV	1.1	1.0	n.a.	n.a.
R.1	W152L, E484K, D624G, G769V	Lentivirus	2.4	4.1	n.a.	n.a.
	W152L	Lentivirus	1.2	2.5	n.a.	n.a.
	E484K	VSV	2.7	1.8	17.0	5.8
	D624G		n.a.	n.a.	n.a.	n.a.
	G769V		n.a.	n.a.	n.a.	n.a.
A.23.1	F157L, V367F, Q613H, D614G, P681R	Lentivirus	0.3	8.2	n.a.	n.a.
	F157L		n.a.	n.a.	n.a.	n.a.
	V367F		n.a.	n.a.	n.a.	n.a.
	Q613H		n.a.	n.a.	n.a.	n.a.
	D614G	VSV	2.4	2.8	n.a.	n.a.
	P681R		n.a.	n.a.	n.a.	n.a.
B.1.617 / India	T95I, G142D, E154K, L452R, E484Q, D614G, P681R, Q1071H	Lentivirus	2.0	n.a.	n.a.	n.a.
	G142D, E154K, V382L, L452R, E484Q, D614G, P681R, Q1071H, D1153Y	Lentivirus	1.9	n.a.	n.a.	n.a.
	T95I	Lentivirus	0.9	2.2	n.a.	n.a.
	G142D		n.a.	n.a.	n.a.	n.a.
	E154K		n.a.	n.a.	n.a.	n.a.
	L452R	Lentivirus	0.5	1.4	n.a.	n.a.
	E484Q	Lentivirus	2.3	2.1	n.a.	n.a.
	D614G	VSV	2.4	2.8	n.a.	n.a.
	P681R		n.a.	n.a.	n.a.	n.a.
	Q1071H		n.a.	n.a.	n.a.	n.a.

B.1.618 / India	del145	VSV	2.1	9.7	1.9	3.9
	del146		n.a.	n.a.	n.a.	n.a.
	E484K	VSV	2.7	1.8	17.0	5.8
	D614G	VSV	2.4	2.8	n.a.	n.a.

Virus	Description	Assay Type	Authentic SARS CoV-2 Neutralizaiton Assay IC_{50} [ng/mL]		
			MP0420	MP0423	
Reference	(French isolate: V367F; E990A)	Authentic	1.3	5.9	
B.1.1.7 / UK	H69_V70del, Y145del, N501Y, A570D, D614G, P681H, T716I, S982A, D1118H	Authentic	1.3	20	
B.1.351 / South Africa	L18F, D80A, D215G, L242_L244del, T302T, K417N, E484K, N501Y, D571D,D614G, A701V	Authentic	7.5	>100	
P.1 / Brazil	L18F, T20N, P26S, D138Y, R190S, K417T, E484K, N501Y, D614G, H655Y, T1027I, V1176F	Authentic	5.7	73	

n.a.: not assessed
Blue shade: no or marginal loss in neutralization potency by therapeutics
Yellow shade: IC_{50} values between 10-100 ng/mL (in a therapeutically active range)
Red shade: IC_{50} values >100 ng/mL (outside therapeutically active range)

263

264 **Table 1b: Summary of the neutralizing efficacy of multispecific DARPin® ensovibep and its monovalent**
265 **RBD-binding DARPin® domains against VSV-SARS-CoV-2 pseudoviruses carrying spike mutants.** The spike
266 variants and mutations were incorporated into VSV-pseudoviruses encoding luciferase as reporter
267 gene. Neutralization tests for multispecific DARPin® ensovibep as well as the mono-valent DARPin®
268 domains RBD-1, RBD-1, RBD-3 were performed and IC_{50} (ng/mL) values are shown for each condition.

Lineage (Origin)	Variants and Point Mutations analyzed	VSV Pseudotype Neutralization Assay IC_{50} [ng/mL]			
		MP0420	Mono-valent RBD Binders in MP0420		
			RBD-1	RBD-2	RBD-3
Reference	Wuhan wild type	1.0	7.3	2.1	13.4
B.1.1.7 / United Kingdom	69-70 del, del145, N501Y, A570D, D614G, P681H, T716I, S982A, D1118H	1.7	4.6	5.4	17.7
	69-70 del, del145, E484K, N501Y, A570D, D614G, P681H, T716I, S982A, D1118H	3.2	**51**	**12.0**	**>100**
	del69-70	1.9	9.3	4.8	22.6
	del145	2.1	7.2	4.9	20
	N501Y	0.6	2.2	9.0	12.6
	A570D	1.2	0.7	0.8	9.8
	D614G	2.4	12.0	6.2	23.0
	P681H	1.5	11.0	4.1	13.0
	T716I	0.6	9.9	3.8	8.9
	S982A	2.0	24.7	7.6	19.8
	D1118H	2.6	5.5	4.6	17.7
B.1.351 / South Africa	D80A, D215G, E484K, N501Y, A701V	5.5	**76**	**26**	**>100**
	L18F, D80A, D215G, Del242-244, R246I, K417N, E484K, N501Y, D614G, A701V	5.0	**38**	2.5	**>100**
	L18F	3.5	8.4	7.2	18.9
	D80A	3.6	9.0	5.8	37.0
	D215G	4.6	11.2	5.1	36.8
	del242-244	2.0	11.2	5.7	8.9
	R246I	1.3	6.3	3.7	17.0
	K417N	0.6	1.2	1.1	4.5
	E484K	2.7	**64.0**	**10.2**	**>100**
	N501Y	0.6	2.2	9.0	12.6
	D614G	2.4	12.0	6.2	23.0
	A701V	1.1	6.3	4.3	27.2

P.1 / Brazil	L18F, T20N, P26S, D138Y, R190S, K417T, E484K, N501Y, D614G, H655Y, T1027I, V1176F	1.2	**31.2**	2.5	**90**
	L18F	3.5	8	7.2	18.9
	T20N	4.6	11.1	7.9	**70**
	P26S	1.8	7.1	**11.8**	17
	D138Y	2.2	13.5	4.8	23.3
	R190S	1.7	9.4	7.4	27.0
	K417T	0.5	4.4	0.6	12.8
	E484K	2.7	**64.0**	**10.2**	**>100**
	N501Y	0.6	2.2	9.0	12.6
	D614G	2.4	12.0	6.2	23.0
	H655Y	2.4	6.3	6.7	13.8
	T1027I	3.3	4.3	5.3	12.2
Individual Mutations	Highly frequent mutations				
S477N	Wide global spread	1.9	3.0	2.0	9.0
N439K	Wide spread in northern amerika, UK; increases RBD/ACE2 interaction[1]	1.3	7.3	5.3	12.9
A222V	Wide European spread	2.2	3.3	4.6	19.5
Individual Mutations	Within RBD epitope of DARPins or reported resistance mutation for other therapeutics				
K417E	residue mutated to N/T in SA, BRA variants	0.5	1.8	1	3.6
G446V		1.7	0.7	1.8	2.3
Y453F	Key residue evolved in Danish mink farms variants	3.2	10.9	5.9	3.3
G476S		1.5	2.3	3.7	29
T478I		2.7	11.2	3.1	16.7
P479S		2.1	7.2	2.3	27.6
V483A		2.3	21.8	8.4	21.3
F486V	Reduces RBD/ACE2 interaction[1]; Key residue for DARPin RBD binder[2]	>100	**>100**	**>100**	**>100**
Q493K		7.9	30	**28.2**	45.8
F490S	Reduces RBD/ACE2 interaction[1]	3.8	2.3	1.7	8.1

Blue shade: no or marginal loss in neutralization potency by ensovibep
Red shade: IC_{50} values for ensovibep >100 ng/mL (outside therapeutically active range)
Bold font >5-fold loss in IC_{50} of mono-valent RBD binders (compared to wild type)
[1] Influence of residue mutations on spike protein binding to human ACE2 (Yi et al. 2020)
[2] Predicted interaction residue for DARPin RBD binder (Walser et al. 2020)

270 **Table 1c: Summary of the neutralizing efficacy of multispecific DARPin® ensovibep and MP0423 and**
271 **monoclonal antibodies REGN10933 and REGN10987 against VSV-SARS-CoV-2 pseudoviruses carrying**
272 **spike mutants.** The spike variants and mutations were incorporated into VSV-pseudoviruses encoding
273 luciferase as reporter gene. Neutralization tests for multispecific DARPin® candidates or monoclonal
274 antibodies were performed and IC_{50} (ng/mL) values are shown for each condition.

Variants	Rational	VSV Pseudotype Neutralizaiton Assay IC_{50} [ng/mL]			
		MP0420	MP0423	REGN10933	REGN10987
Reference	Wuhan wild type	1.0	3.1	3.9	6.0
Individual Mutations	Highly frequent mutations				
S477N	Wide global spread	1.9	0.8	n.a	n.a
N439K	Wide spread in northern amerika, UK; increases RBD/ACE2 interaction[1]	1.3	2.5	2.8	30.1
A222V	Wide European spread	2.2	3.1	7.00	2.9
Individual Mutations	Within RBD epitope of DARPins or reported resistance mutation for other therapeutics				
K417E	Residue mutated to N/T in SA, BRA variants	0.5	1.2	>100	1.5
G446V	Key residue evolved in Danish mink farms variants	1.7	1.0	1.5	>100
Y453F		3.2	2.0	>100	11.8
G476S		1.5	3.1	n.a	n.a
T478I		2.7	2.8	4.0	7.0
P479S		2.1	1.5	3.7	9.8
V483A		2.3	1.9	n.a	n.a
F486V	Reduces RBD/ACE2 interaction[1] Key residue for DARPin RBD binder[2];	>100	7.7	>100	4.4
Q493K		7.9	2.4	>100	10
F490S	Reduces RBD/ACE2 interaction[1]	3.8	1.6	3.1	9.2

n.a.: not assessed
Blue shade: no or marginal loss in neutralization potency by therapeutics
Yellow shade: IC_{50} values between 10-100 ng/mL (in a therapeutically active range)
Red shade: IC_{50} values >100 ng/mL (outside therapeutically active range)
[1] Influence of residue mutations on spike protein binding to human ACE2 (Yi et al. 2020)
[2] Predicted interaction residue for DARPin RBD binder (Walser et al. 2020)

275

Supplementary Materials for

Multispecific DARPin® therapeutics demonstrate very high potency against SARS-CoV-2 variants

Rothenberger et al. 2021

291 # Materials and Methods

292

293 *Generation of His-tagged mono-valent RBD binders, ensovibep, MP0423 and the domain k.o. variants of*
294 *MP0423*

295 DARPin® constructs selected and cloned as described in Walser et al.[20] were transformed in *E.coli* BL21
296 cells, plated on LB-agar (containing 1% glucose and 50 µg/ml ampicillin) and then incubated overnight
297 at 37°C. A single colony was picked into TB medium (containing 1% glucose and 50 µg/ml ampicillin)
298 and incubated overnight at 37°C, shaking at 230 rpm. Fresh TB medium (containing 50 µg/ml ampicillin)
299 was inoculated with 1:20 of overnight culture and incubated at 37°C at 230 rpm. At OD600 = 1.1 the
300 culture was induced by addition of IPTG (0.5 mM final concentration) and incubated further for 5 h at
301 37°C and 230 rpm. Harvest was done by centrifugation (10 min 5000 x g). After cell disruption by
302 sonication, primary recovery was done by heat treatment for 30 min at 62.5°C and subsequent
303 centrifugation (15 min, 12000 x g). 20 mM Imidazole and 1% Triton X-100 was added to the supernatant
304 and the 0.22 µm filtered supernatant was further purified by immobilized metal affinity
305 chromatography (IMAC) (HisTrap FF crude, Cytiva, Sweden) using the N-terminal His-tag and including
306 a wash step with 1% Triton X-100 and a step elution with 250 mM Imidazole. In a subsequent step, the
307 elution fraction of the IMAC step was applied on a size exclusion chromatography (Superdex 200,
308 Cytiva, Sweden) and fractions of interest were pooled and concentrated. Finally, the concentrated
309 sample was filtered through a 0.22 µm Mustang E filter for Endotoxin removal and sterile filtration and
310 quality controlled.

311

312 *Generation of monoclonal antibodies, REGN10933, REGN10987 and S309*

313 Publicly available sequences of variable domains from monoclonal antibodies RGN10933, RGN10987
314 (WHO Drug Information, Vol. 34, No. 3, 2020, Proposed INN: List 124 – COVID-19) and S309 (PDB:
315 6WPS) were used to synthetize the corresponding cDNA fragments and cloned into a proprietary
316 expression vector at Evitria AG (Switzerland). Generated vectors containing the constant
317 immunoglobulin hIgG1 chain or kappa light chain were used for transfection in Chinese hamster ovary
318 cells by Evitria. Sterile filtered cell supernatants were purified via affinity purification with HiTrap
319 MabSelect column followed by a size exclusion chromatography using HiLoad 26/600 Superdex 200
320 column in PBS pH7.4. Selected fractions were pooled and quality controlled (by SDS-PAGE, size
321 exclusion chromatography and endotoxin measurement), before use in assays.

322

323

324 *VSV-SARS-CoV-2 pseudotype mutation-vector generation*

325 Plasmid pCAGGS containing the spike protein of SARS-CoV-2[20] was used as template for generation of
326 single and multiple spike protein mutants. Forward and reverse complementary primers encoding the
327 mutation were synthesized by Microsynth (Balgach, Switzerland). High-fidelity Phusion polymerase
328 (New England Biolabs, USA) was used for all DNA amplification.

329 Single mutations of the spike protein were generated via two PCR fragments of the spike ORF using
330 high-fidelity Phusion polymerase (New England Biolabs, USA). The first fragment was generated via a
331 generic forward primer (pCAGGS-5) annealing upstream of the spike ORF and the specific reverse
332 primer encoding the mutation. The second fragment was generated using the specific forward primer
333 encoding the mutation and a reverse primer (rbglobpA-R). The two fragments were gel-purified and
334 used as input for an assembly PCR without addition of flanking primers.

335 For multi-mutation spike proteins, a complementary pair of primers (forward and reverse) encoding
336 each mutation was designed. Fragment 1 was generated with forward primer pCAGGS-5 and reverse
337 primer encoding mutation 1. Fragment 2 was generated using forward primer encoding mutation 1 and
338 reverse primer encoding mutation 2. All subsequent fragments were generated analogously. DNA
339 fragments were gel-purified and mixed in equimolar amounts. This mix was used for re-assembly of the
340 full spike ORF using outer primers pCAGGS-5 and rbglobpA-R.

341 For both single as well as multi-mutation spike protein, the full-length spike ORF was isolated from an
342 agarose gel, digested by restriction enzymes NheI/EcoRI and inserted into the pCAGGS vector
343 backbone. The correct sequence was verified via sequencing the whole ORF of the spike protein by
344 Microsynth (Balgach, Switzerland).

345

346 *VSV-SARS-CoV-2 pseudotype neutralization assay for mutational analysis and MP0423 domain knock outs*

347 The pseudotype viral system was based on the recombinant VSV*ΔG-Luc vector in which the
348 glycoprotein gene (G) had been deleted and replaced with genes encoding green fluorescent protein
349 and luciferase[30]. Pseudoviruses were generated as reported previously[31,32]. For the neutralization assay,
350 an initial dilution of the compounds was followed by three-fold dilutions in quadruplicates in DMEM-2
351 % [vol/vol] FCS supplemented with 20 µM human serum albumin (CSL Behring). The mixture was mixed
352 with an equal volume of DMEM-2 % FCS containing 250 infectious units (IU) per well of SARS-CoV-2
353 pseudoviruses and incubated for 90 min at 37°C. The mix was inoculated onto Vero E6 cells[33,34] in a
354 clear bottom white walled 96-well plate during 90 min at 37°C. The inoculum was removed and fresh
355 medium added, and cells further incubated at 37°C for 16 h. Cell were lysed according to the ONE-Glo™
356 luciferase assay system (Promega, Madison, US) and light emission was recorded using a Berthold®
357 TriStar LB941 luminometer. The raw data (relative light unit values) were exported to GraphPad Prism

358 v8.4.3, and the % neutralization values were normalized to the untreated PsV signal. IC_{50} with 95%
359 confidence interval were estimated by model of nonlinear regression fit with settings for log (inhibitor)
360 vs normalized response curves. Data points are plotted by the mean ± SEM (standard error of mean).
361
362 SARS-CoV-2 lentivirus-based pseudovirus neutralization assay
363 The neutralizing activity of therapeutic antibodies against SARS-COV-2 variants was measured using
364 lentiviral particles pseudotyped with spike proteins of SARS-COV-2 variants, as previously described[35].
365 Briefly, pseudoviruses bearing the spike proteins and carrying a firefly luciferase (FLuc) reporter gene
366 were produced in 293T cells by co-transfection of pCMVΔR8.2, pHR'CMVLuc and pCDNA3.1(+)-spike
367 variants. Plasmids encoding human codon-optimized spike genes with the desired mutations were
368 purchased (GenScript, Piscataway, NJ). Supernatants containing pseudoviruses were collected 48 h
369 post-transfection, filtered through a 0.45 µm low protein binding filter, and stored at -80°C. Pseudovirus
370 titers were measured by infecting 293T-ACE2.TMPRSS2s cells for 48 h prior to measuring luciferase
371 activity (luciferase assay reagent, Promega, Madison, WI). For neutralization assays, pseudoviruses with
372 titers of approximately 10^6 relative luminescence units (RLU)/ml were incubated with serially diluted
373 antibodies for two h at 37°C before adding the pseudovirus and antibody mixtures (100 µl) onto 96 well
374 plates pre-seeded one day earlier with 3.0 x 10^4 293T-ACE2.TMPRSS2s cells/well. Pseudovirus infection
375 was scored 48 h later by measuring luciferase activity. The antibody concentration causing a 50%
376 reduction of RLU compared to control (ID_{50}) was reported as the neutralizing antibody titer. Titers were
377 calculated using a nonlinear regression curve fit (GraphPad Prism software Inc., La Jolla, CA). The ratio
378 of the neutralizing antibody titer of the variant compared to the neutralizing antibody titer of wild type
379 was calculated. The mean titer from at least two independent experiments with intra-assay duplicates
380 was reported as the final titer. This work was performed independently by investigators at the US Food
381 and Drug Administration, Center for Biologics Evaluation and Research as part of Therapeutics Research
382 Team for the US government COVID-19 response efforts.
383
384 *Cells and pathogenic virus*
385 Vero E6 cells (kindly provided by Prof. Volker Thiel, University of Bern, Switzerland) were passaged in
386 Minimum Essential Medium (MEM) (Cat N° M3303) containing 10% fetal bovine serum (FBS) and
387 supplements (2 mM L-Glutamine, 1% Non-essential amino acids, 100 units/ml Penicillin, 100 µg/ml
388 Streptomycin, 0.06% Sodium bicarbonate, all from Bioswisstec, Schaffhausen, Switzerland) at 37°C,
389 >85% humidity and 5% CO_2. Vero E6/TMPRSS2 cells[33,34] obtained from the Centre For AIDS Reagents
390 (National Institute for Biological Standards and Control) were passaged in Dulbecco's Modified Eagle
391 Medium (DMEM) (Cat N° M1452) containing 10% fetal bovine serum (FBS) and supplements (2 mM L-

392 Glutamine, 1% Non-essential amino acids, 100 U/ml Penicillin, 100 µg/ml Streptomycin, 0.06% Sodium
393 bicarbonate and 2% Geneticin G418 , all from Bioswisstec, Schaffhausen, Switzerland) at 37°C, >85%
394 humidity and 5% CO_2.
395 SARS-CoV-2 (2019-nCoV/IDF0372/2020), kindly provided by Dr. Sylvie van der Werf from the National
396 Reference Centre for Respiratory Viruses hosted by Institut Pasteur (Paris, France) was propagated in
397 Vero E6 cells in MEM containing 2% FBS and supplements (2%-FBS-MEM) at 37°C, >85% humidity and
398 5% CO_2. SARS-CoV-2 variants (B.1.1.7, B.1.351 and P.1) were provided from University Hospital of
399 Geneva, Laboratory of Virology (HUG) and propagated in Vero E6/TMPRSS2 cells in DMEM containing
400 2% FBS and supplements (2%-FBS-DMEM) at 37°C, >85% humidity and 5% CO_2. Viral titer was
401 determined by standard plaque assay, by incubating 10-fold serial dilutions of the virus for 1 h at 37°C
402 on a confluent 24-well plate with Vero E6 cells. Then inoculum was removed and 1 ml overlay medium
403 (20 ml Dulbecco's Modified Eagle's Medium, 5 ml FBS, 100 U/ml Penicillin, 100 µg/ml Streptomycin,
404 and 25 ml Avicel rc581) was added. After 3 days incubation at 37°C the overlay was removed and the
405 plates stained with crystal violet solution (spatula tip (~4 mg) crystal violet powder (Sigma Aldrich)
406 solved in 30 ml 37% formalin and 120 ml PBS (Sigma Aldrich).
407
408 *Viral passaging experiment with authentic SARS-CoV-2*
409 Virus escape studies were adapted from a previously published protocol by Baum et al.[13]. Briefly, 1:5
410 serial dilutions of DARPin® antivirals and monoclonal antibodies from 100 µg/mL to 0.032 µg/mL were
411 prepared in Minimum Essential Medium (MEM) containing 2% FBS, supplements and 10 µM human
412 serum albumin (HSA; CSL Behring, Switzerland; 2%-FBS-MEM + HSA). 500 µl of virus suspension
413 containing 1.5 x 10^6 plaque forming units (pfu) SARS-CoV-2 in 2%-FBS-MEM + HSA were mixed with 500
414 µl of serially diluted DARPin® molecules or monoclonal antibodies and subsequently incubated for 1
415 hour at 37°C. The mixtures were then transferred to confluent Vero E6 cells in 12 well plates and
416 incubated for 4 days at 37°C, >85% humidity and 5% CO_2. Each culture well was assessed for cytopathic
417 effect (CPE) by microscopy. Supernatant was removed from wells with the highest DARPin® or antibody
418 concentrations showing significant CPE (≥20%) and used for total RNA extraction and further passaging.
419 For subsequent rounds of passaging, remaining 900 µl supernatant of selected wells was diluted in 4
420 ml in 2%-FCS-MEM + HSA and from the 4.9 mL, 500 µl mixed with serial dilutions of DARPin® molecules
421 or antibodies, incubated and the mixture transferred to 12-well plates with fresh Vero E6 cells as
422 described above. Cell culture wells were assessed for CPE again after 4 days and the supernatant of
423 wells with highest DARPin® or antibody concentrations with evident viral replication (CPE) harvested
424 and used for additional passages. A total of 4 passages were performed this way.
425 Deep sequencing of viral passages

426 RNA of the cell culture supernatant was extracted using the RNeasy Universal Plus kit (Qiagen, Basel,
427 Switzerland) according to the manufacturer's protocol. 10.5 µl of the extract was reverse transcribed
428 using Superscript VILO (ThermoFisher Scientific, Reinach, Switzerland) following the manufacturer's
429 instructions. Barcoded libraries were prepared on the Ion Chef Instrument (ThermoFisher Scientific)
430 using the Ion AmpliSeq SARS-CoV-2 Research Panel (ThermoFisher Scientific). 8-16 barcoded samples
431 were pooled and loaded on one Ion 530 chip using the Ion Chef Instrument (ThermoFisher Scientific)
432 and sequenced on the Ion S5 System with 550 flows.
433 The resulting BAM files were converted to fastq format using Samtools 1.10[38] and subjected to adapter
434 and quality trimming using Trimmomatic 0.39[39] (options: ILLUMINACLIP:adapters.fasta:2:30.10,
435 LEADING: 3, TRAILING: 3, SIDINGWINDOW:4:15, MINLEN:36). Reads were aligned to the SARS-CoV-2
436 reference genome (NC_045512.2) using bwa 0.7.17[40] and variants were determined using LoFreq
437 v2.1.5[41]. Variants were filtered for a minimal depth (DP) of 400X and a minimal allele frequency (AF) of
438 3% using bcftools 1.10[38]. Functional annotation of the variants was performed using SNPEff 5.0[42].
439 Variants were visualized in R 3.6.1[43] using ComplexHeatmap 2.2[44].
440
441 *Virus neutralization of authentic wild type and variants of SARS-CoV-2 determined by Cell Titer-Glo*
442 Virus neutralization capacity of mono-valent DARPin® candidate and multispecific DARPin® molecules
443 was determined for 100 $TCID_{50}$ SARS-CoV-2 variants from lineage B.1.1.7 (H69_V70del, Y145del,
444 N501Y, A570D, D614G, P681H, T716I, S982A, D1118H), B.1.351 (L18F, D80A, D215G, L242_L244del,
445 T302T, K417N, E484K, N501Y, D571D,D614G, A701V) and P.1 (L18F, T20N, P26S, D138Y, R190S,
446 K417T, E484K, N501Y, D614G, H655Y, T1027I, V1176F) in reference to a wild-type French isolate (with
447 the following differences to the Wuhan wild-type: V367F; E990A) by measuring ATP levels of
448 protected cells in a cell viability assay. DARPin® molecules were serially diluted 1:4 from 40 nM to 2.4
449 pM (in triplicates) in 100 µl cell culture medium (2%-FBS-DMEM) enriched with 10 µM HSA in 96 well
450 plates. The diluted DARPin® antivirals were mixed with 100 $TCID_{50}$ SARS-CoV-2 in 100 µl 2%-FBS-MEM
451 + HSA and incubated for 1 h at 37°C. DARPin®/virus mixtures (200 µl) were transferred onto confluent
452 Vero E6/TMPRSS2. The controls consisted of cells exposed to virus suspension only, to determine
453 maximal cytopathic effect and of cells incubated with medium only, to determine baseline state of
454 cells. The plates were incubated for 3 days at 37°C, >85% humidity and 5% CO_2. Cell viability was
455 determined by removing 100 µl supernatant from all wells and adding 100 µl CellTiter-Glo reagent to
456 the cells as described in the manufacturers protocol (CellTiter-Glo® Luminescent Cell Viability Assay,
457 Promega, Madison, USA). After 2 minutes shaking on an orbital shaker, lysis of the cells during 10 min
458 and transfer to an opaque-walled plate at room temperature, luminescence was read using a GloMax
459 instrument (Promega).

460

461 *Neutralization of authentic SARS-CoV-2 by MP0423 and its domain knock-outs was determined by Cell*
462 *Titer-Glo and real-time RT-PCR*

463 Virus neutralization capacity of mono-valent DARPin® candidate and multispecific DARPin® molecules
464 was determined for 100 $TCID_{50}$ SARS-CoV-2 wild-type French isolate (with the following differences to
465 the Wuhan wild-type: V367F; E990A) by measuring ATP levels of protected cells in a cell viability assay.
466 DARPin® molecules were serially diluted 1:4 from 40 nM to 2.4 pM (in triplicates) in 100 µl cell culture
467 medium (2%-FBS-MEM) enriched with 10 µM HSA in 96 well plates. The diluted DARPin® molecules
468 were mixed with 100 $TCID_{50}$ SARS-CoV-2 in 100 µl 2%-FBS-MEM + HSA and incubated for 1 h at 37°C.
469 DARPin®/virus mixtures (200 µl) were transferred onto confluent Vero E6 cells. The controls consisted
470 of Vero E6 cells exposed to virus suspension only, to determine maximal cytopathic effect and of cells
471 incubated with medium only, to determine baseline state of cells. The plates were incubated for 3 days
472 at 37°C, >85% humidity and 5% CO_2. Cell viability was determined by removing 100 µl supernatant from
473 all wells and adding 100 µl CellTiter-Glo reagent as described in the manufacturers protocol (CellTiter-
474 Glo® Luminescent Cell Viability Assay, Promega, Madison, USA). Luminescence was read after 2 minutes
475 shaking on an orbital shaker, transferring the mixture to an opaque-walled plate and 10 min incubation
476 at room temperature using the GloMax instrument (Promega). To measure virus replication, the
477 previously removed supernatant (100 µl) was inactivated in 400 µl AVL-buffer (Qiagen, Hilden,
478 Germany) and 400 µl 100% ethanol and extracted using the MagNAPure 96 system (Roche, Basel,
479 Switzerland) and eluted in 100 µl. Viral RNA was quantified by real-time RT-PCR targeting the E gene
480 (Eurosurveillance | Detection of 2019 novel coronavirus (2019-nCoV) using 5 µl RNA and 20 µl TaqMan
481 Fast Virus 1-Step Master Mix (Life Technologies, Zug, Switzerland). Viral genome equivalents (ge) were
482 calculated using a regression analysis and an internal standard.

483 ## Supplementary Figures

484

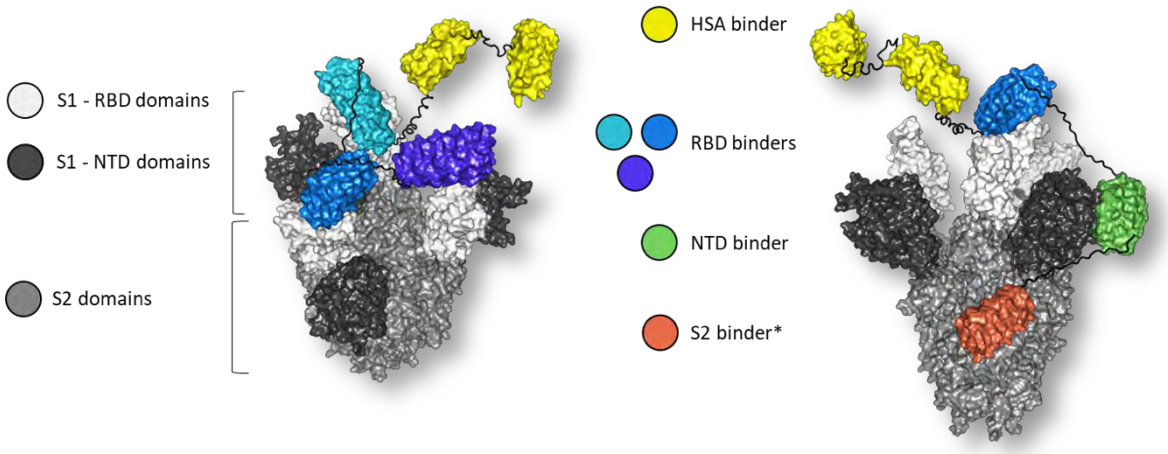

485
486 **Supplementary Figure 1:** Molecular model of multispecific DARPin® antivirals.
487 Molecular model of multi-paratopic DARPin® candidate ensovibep (left) consisting of five DARPin®
488 domains (yellow: HSA-binding domains, shades of blue: RBD-binding domains) bound to the RBDs
489 (white) of the spike ectodomain (grey). Linkers are shown in black. Position of RBD and NTD binders
490 guided by Cryo-EM data. Molecular model of multispecific MP0423 (right), consisting of five DARPin®
491 domains (yellow: HSA-binding domains, blue: RBD-binding domain, green: NTD-binding domain,
492 orange: S2-binding domain) bound to the spike ectodomain. Linkers are shown in black. *For the S2
493 binder, the epitope is unknown.[20]

494

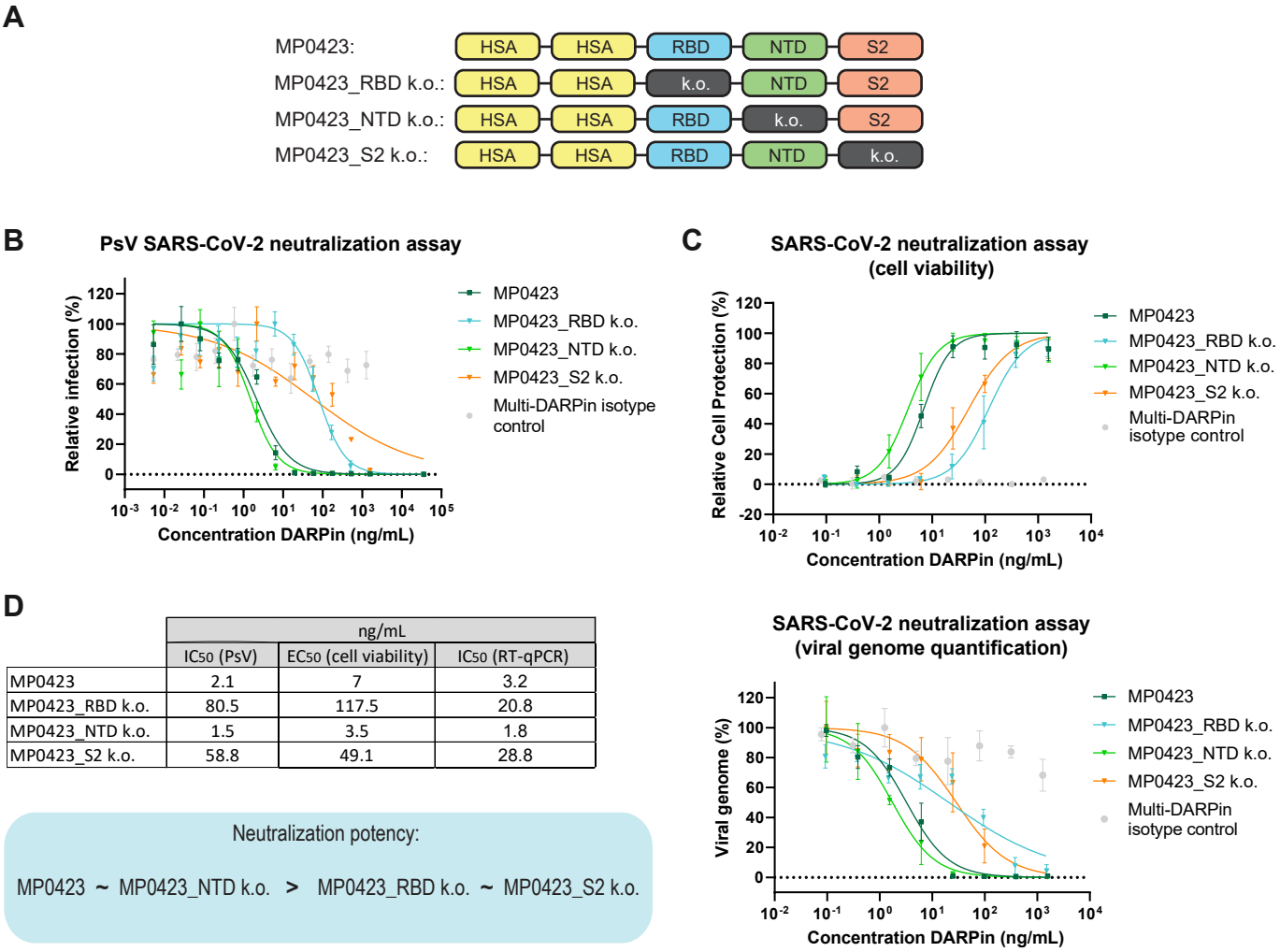

	ng/mL		
	IC50 (PsV)	EC50 (cell viability)	IC50 (RT-qPCR)
MP0423	2.1	7	3.2
MP0423_RBD k.o.	80.5	117.5	20.8
MP0423_NTD k.o.	1.5	3.5	1.8
MP0423_S2 k.o.	58.8	49.1	28.8

Neutralization potency:

MP0423 ~ MP0423_NTD k.o. > MP0423_RBD k.o. ~ MP0423_S2 k.o.

Supplementary Figure 2: Determination of the contribution of the single DARPin® domains of MP0423 in the neutralization activity against SARS-CoV-2. A) Schematic representation of the multi-specific MP0423 knock-out (k.o) constructs. In each k.o. construct, the indicated SARS-CoV-2-binding domain is replaced by a non-binding DARPin®. HSA: HSA-binding DARPin®, RBD: RBD-binding DARPin®, NTD: NTD-binding DARPin®, S2: S2-binding DARPin®; **B)** Neutralization profiles of MP0423 and k.o constructs against VSV-SARS-CoV-2 pseudoviruses expressing the wild-type spike protein; **C)** Upper panel: protective effect of DARPin® molecules against SARS-CoV-2 (100 pfu)-mediated cytopathic effect. Depicted are the percentage of cell protection conferred by MP0423 or the k.o contructs. Cell protection was determined after 3 days of incubation by measuring intracellular ATP levels in a cell viability assay using Cell Titer-Glo. Lower panel: inhibition of SARS-CoV-2 viral replication quantified by real-time RT-PCR and expressed as percentage of viral genome equivalents present in the supernatant of Vero E6 cells exposed to 100 pfu SARS-CoV-2 with increasing amounts of MP0423 or k.o. constructs. **D)** IC_{50}/EC_{50}values and potency ranking of the constructs analyzed. No potency loss compared to MP0423 was observed for MP0423_NTD k.o. while a reduction in neutralization activity was observed for the MP0423_RBD k.o. and the MP0423_S2 k.o. constructs.

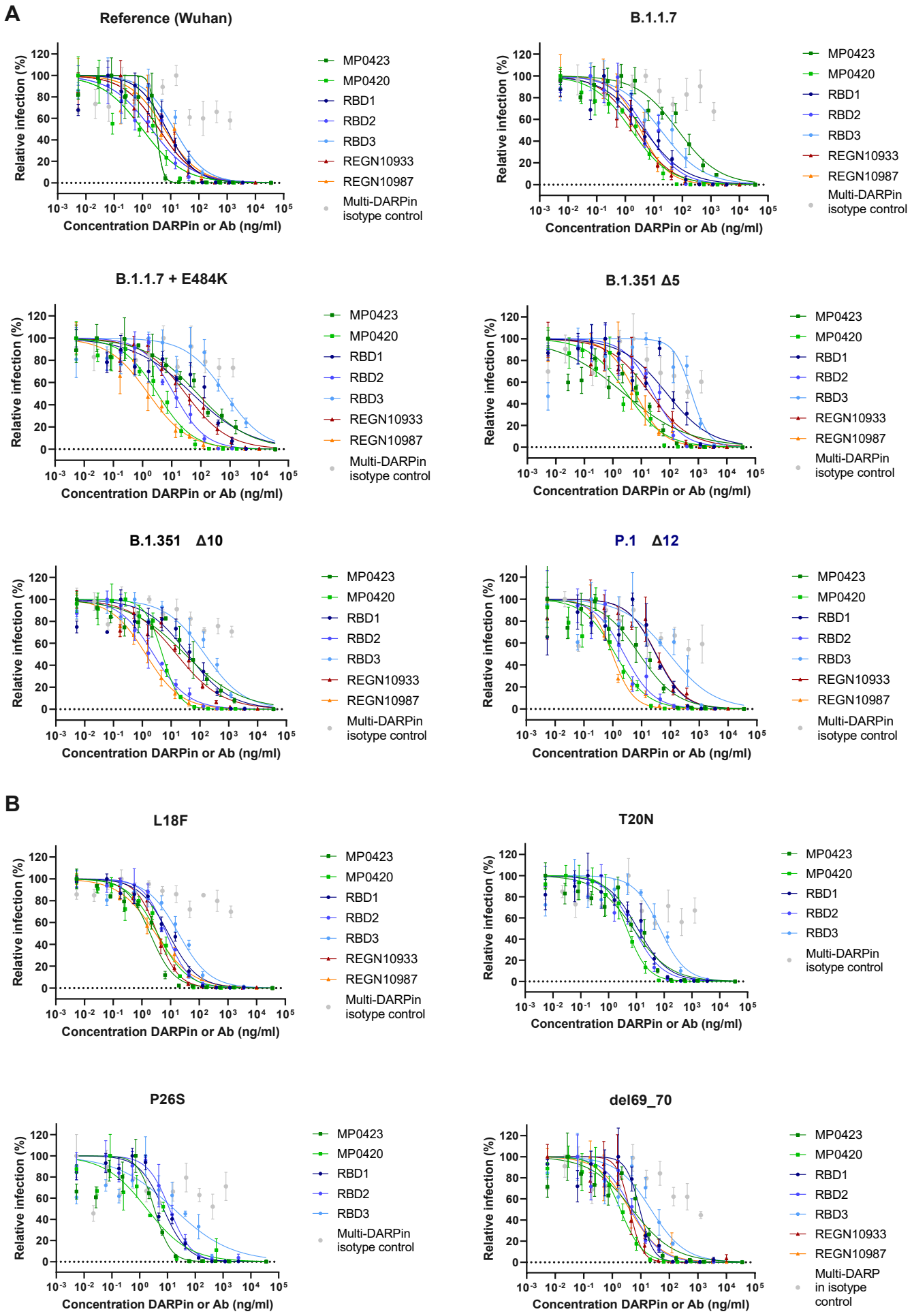
A
Reference (Wuhan)
B.1.1.7
B.1.1.7 + E484K
B.1.351 Δ5
B.1.351 Δ10
P.1 Δ12
B
L18F
T20N
P26S
del69_70
Relative infection (%)
Concentration DARPin or Ab (ng/ml)
MP0423
MP0420
RBD1
RBD2
RBD3
REGN10933
REGN10987
Multi-DARPin isotype control
Multi-DARP in isotype control

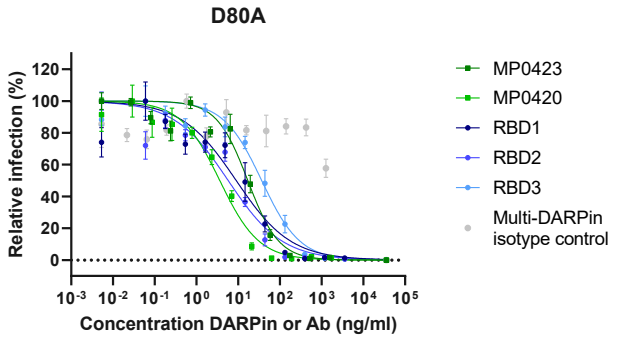
D80A
Relative infection (%)
Concentration DARPin or Ab (ng/ml)
MP0423
MP0420
RBD1
RBD2
RBD3
Multi-DARPin isotype control

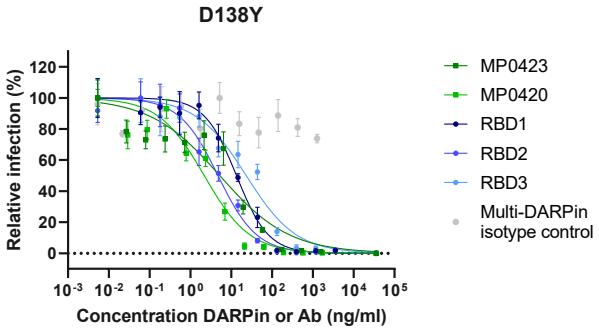
D138Y
Relative infection (%)
Concentration DARPin or Ab (ng/ml)
MP0423
MP0420
RBD1
RBD2
RBD3
Multi-DARPin isotype control

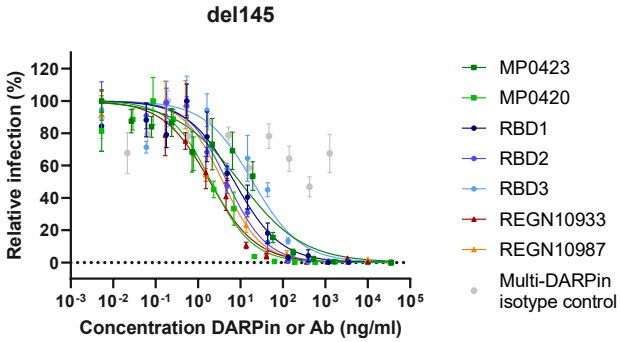
del145
Relative infection (%)
Concentration DARPin or Ab (ng/ml)
MP0423
MP0420
RBD1
RBD2
RBD3
REGN10933
REGN10987
Multi-DARPin isotype control

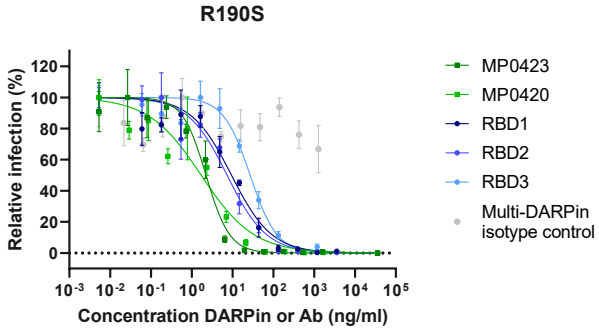
R190S
Relative infection (%)
Concentration DARPin or Ab (ng/ml)
MP0423
MP0420
RBD1
RBD2
RBD3
Multi-DARPin isotype control

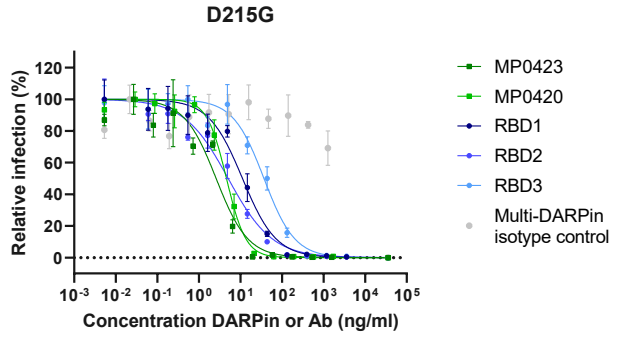
D215G
Relative infection (%)
Concentration DARPin or Ab (ng/ml)
MP0423
MP0420
RBD1
RBD2
RBD3
Multi-DARPin isotype control

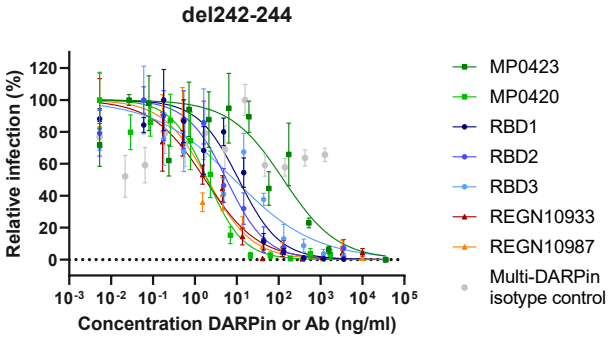
del242-244
Relative infection (%)
Concentration DARPin or Ab (ng/ml)
MP0423
MP0420
RBD1
RBD2
RBD3
REGN10933
REGN10987
Multi-DARPin isotype control

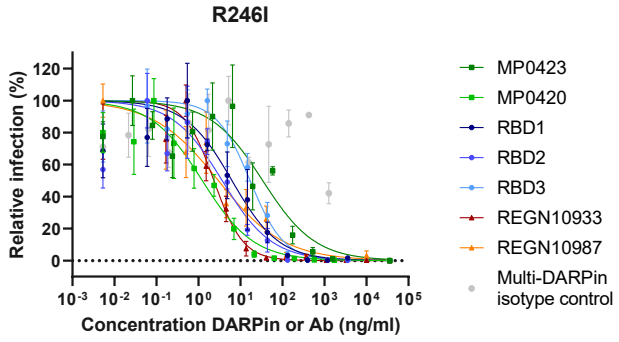
R246I
Relative infection (%)
Concentration DARPin or Ab (ng/ml)
MP0423
MP0420
RBD1
RBD2
RBD3
REGN10933
REGN10987
Multi-DARPin isotype control

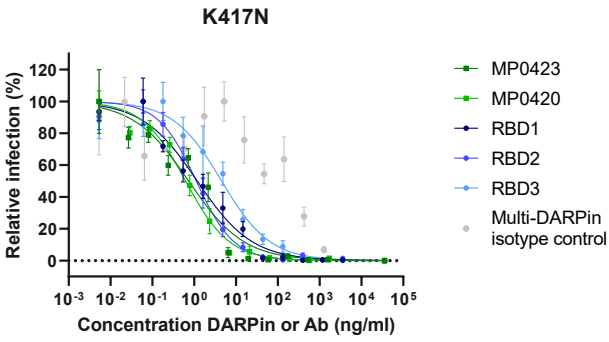
K417N
Relative infection (%)
Concentration DARPin or Ab (ng/ml)
MP0423
MP0420
RBD1
RBD2
RBD3
Multi-DARPin isotype control

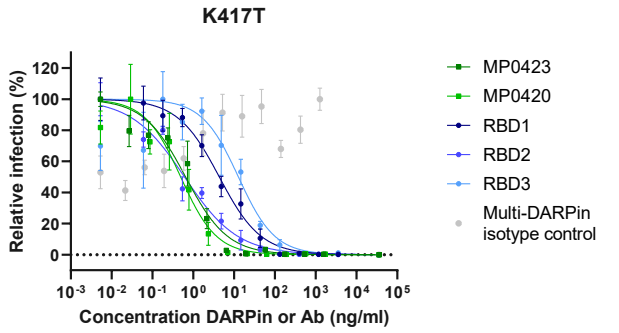
K417T
Relative infection (%)
Concentration DARPin or Ab (ng/ml)
MP0423
MP0420
RBD1
RBD2
RBD3
Multi-DARPin isotype control

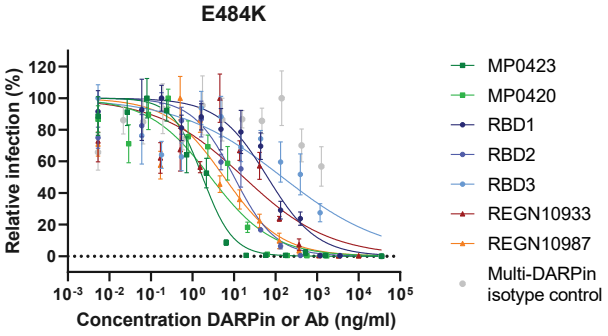
E484K
Relative infection (%)
Concentration DARPin or Ab (ng/ml)
MP0423
MP0420
RBD1
RBD2
RBD3
REGN10933
REGN10987
Multi-DARPin isotype control

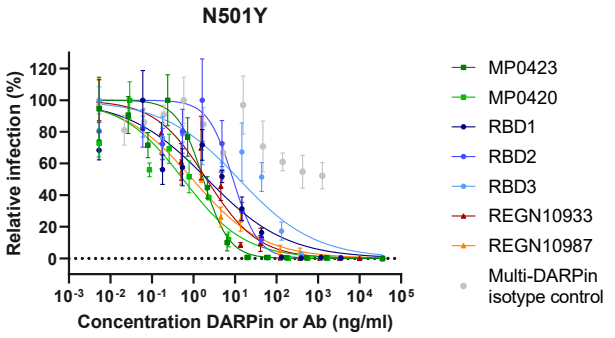
N501Y
Relative infection (%)
Concentration DARPin or Ab (ng/ml)
MP0423
MP0420
RBD1
RBD2
RBD3
REGN10933
REGN10987
Multi-DARPin isotype control

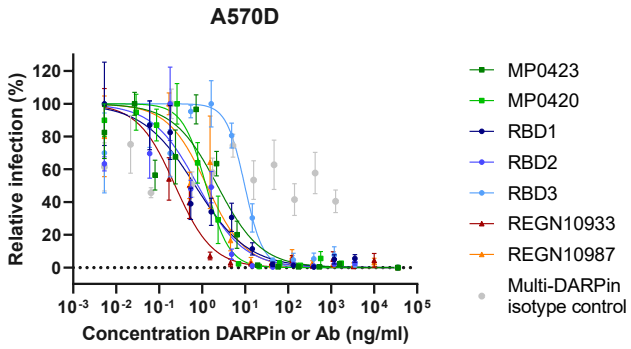
A570D
Relative infection (%)
Concentration DARPin or Ab (ng/ml)
MP0423
MP0420
RBD1
RBD2
RBD3
REGN10933
REGN10987
Multi-DARPin isotype control

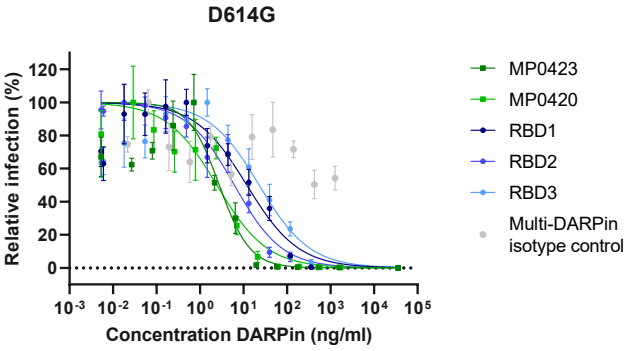
D614G
Relative infection (%)
Concentration DARPin (ng/ml)
MP0423
MP0420
RBD1
RBD2
RBD3
Multi-DARPin isotype control

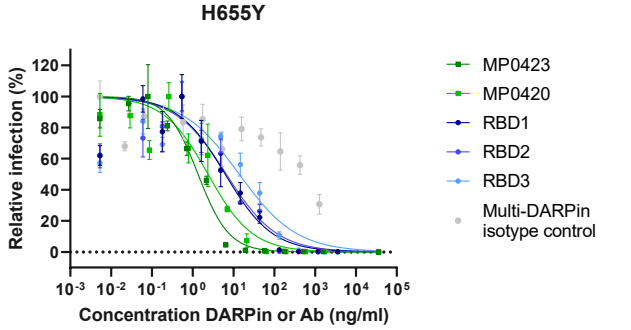
H655Y
Relative infection (%)
Concentration DARPin or Ab (ng/ml)
MP0423
MP0420
RBD1
RBD2
RBD3
Multi-DARPin isotype control

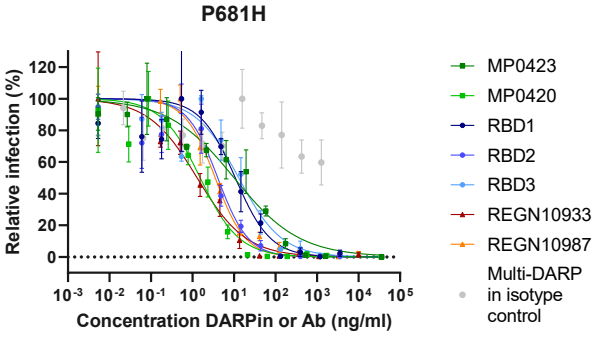
P681H
Relative infection (%)
Concentration DARPin or Ab (ng/ml)
MP0423
MP0420
RBD1
RBD2
RBD3
REGN10933
REGN10987
Multi-DARP in isotype control

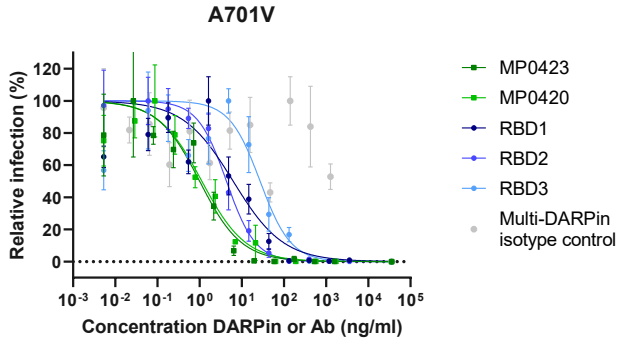
A701V
Relative infection (%)
Concentration DARPin or Ab (ng/ml)
MP0423
MP0420
RBD1
RBD2
RBD3
Multi-DARPin isotype control

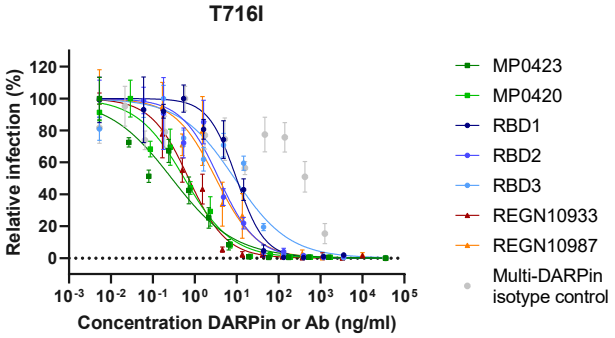
T716I
Relative infection (%)
Concentration DARPin or Ab (ng/ml)
MP0423
MP0420
RBD1
RBD2
RBD3
REGN10933
REGN10987
Multi-DARPin isotype control

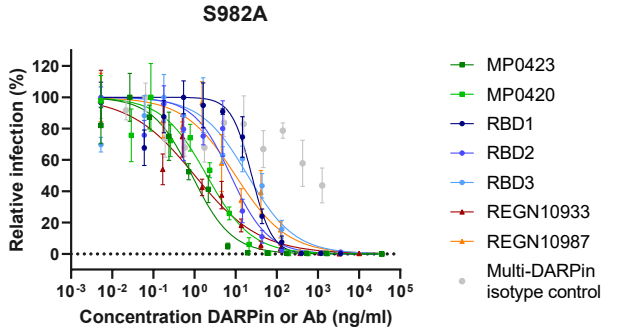
S982A
Relative infection (%)
Concentration DARPin or Ab (ng/ml)
MP0423
MP0420
RBD1
RBD2
RBD3
REGN10933
REGN10987
Multi-DARPin isotype control

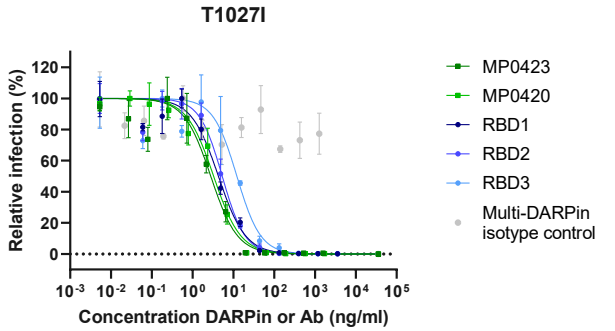
T1027I
Relative infection (%)
Concentration DARPin or Ab (ng/ml)
MP0423
MP0420
RBD1
RBD2
RBD3
Multi-DARPin isotype control

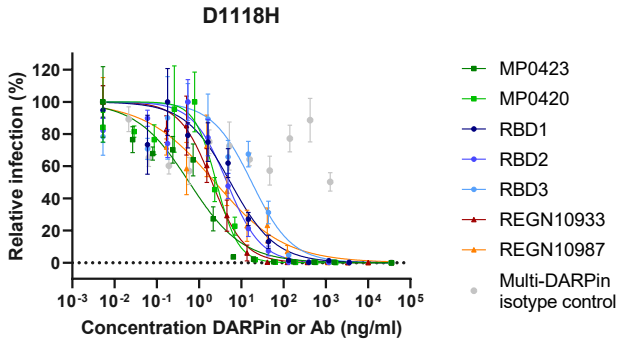
D1118H
Relative infection (%)
Concentration DARPin or Ab (ng/ml)
MP0423
MP0420
RBD1
RBD2
RBD3
REGN10933
REGN10987
Multi-DARPin isotype control

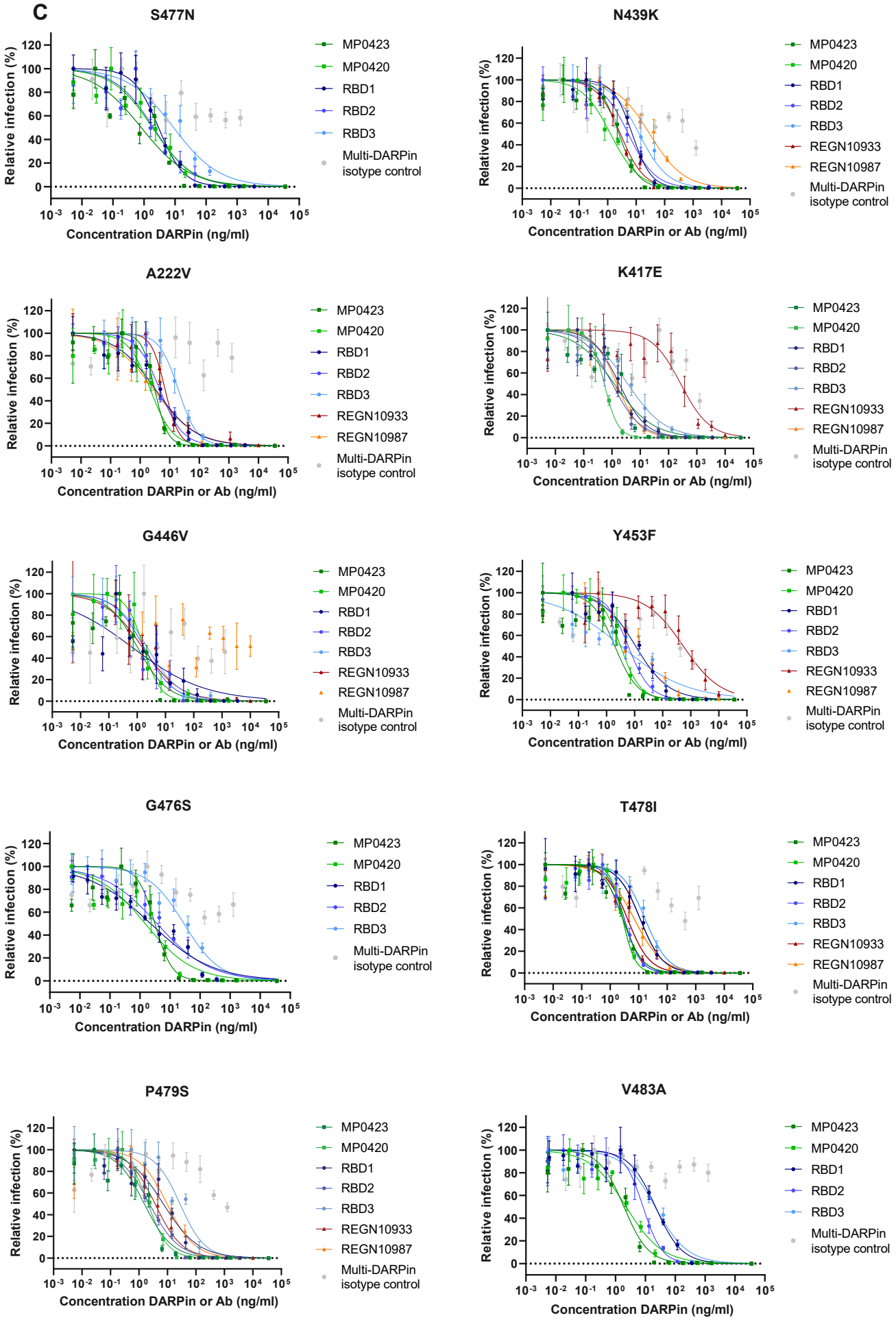
C
S477N
N439K
A222V
K417E
G446V
Y453F
G476S
T478I
P479S
V483A
Relative infection (%)
Concentration DARPin (ng/ml)
Concentration DARPin or Ab (ng/ml)
MP0423
MP0420
RBD1
RBD2
RBD3
REGN10933
REGN10987
Multi-DARPin isotype control

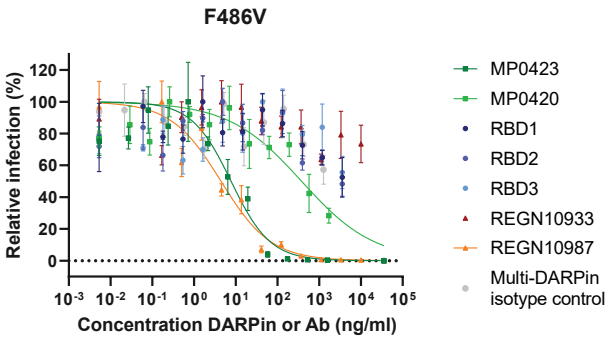
F486V
Relative infection (%)
Concentration DARPin or Ab (ng/ml)
MP0423
MP0420
RBD1
RBD2
RBD3
REGN10933
REGN10987
Multi-DARPin isotype control

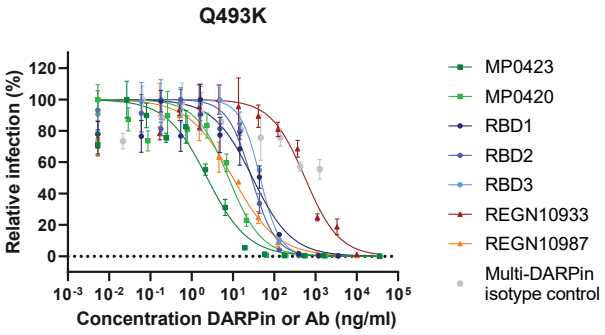
Q493K
Relative infection (%)
Concentration DARPin or Ab (ng/ml)
MP0423
MP0420
RBD1
RBD2
RBD3
REGN10933
REGN10987
Multi-DARPin isotype control

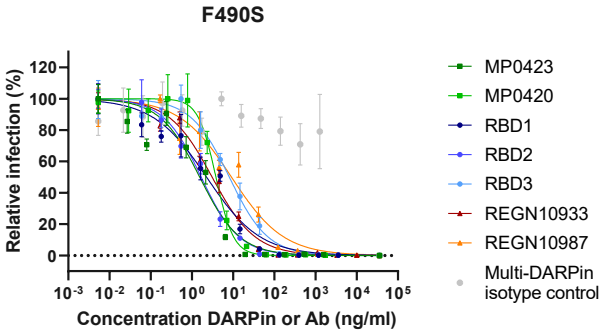
F490S
Relative infection (%)
Concentration DARPin or Ab (ng/ml)
MP0423
MP0420
RBD1
RBD2
RBD3
REGN10933
REGN10987
Multi-DARPin isotype control

D

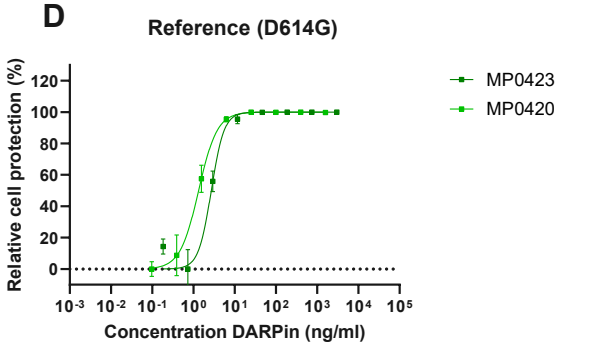
Reference (D614G)
Relative cell protection (%)
Concentration DARPin (ng/ml)
MP0423
MP0420

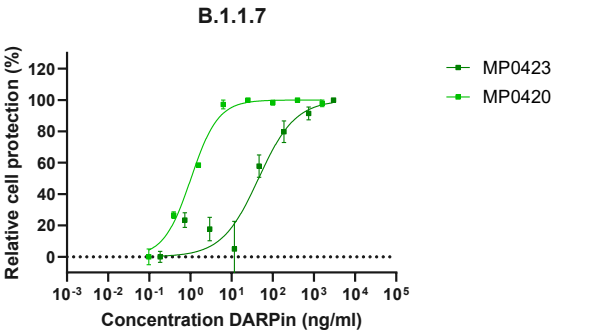
B.1.1.7
Relative cell protection (%)
Concentration DARPin (ng/ml)
MP0423
MP0420

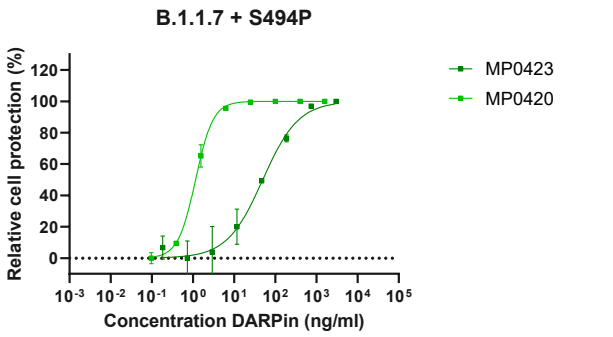
B.1.1.7 + S494P
Relative cell protection (%)
Concentration DARPin (ng/ml)
MP0423
MP0420

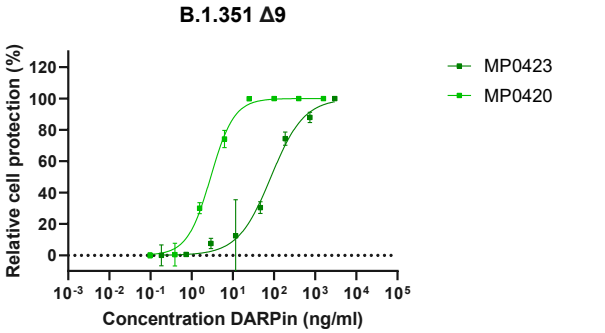
B.1.351 Δ9
Relative cell protection (%)
Concentration DARPin (ng/ml)
MP0423
MP0420

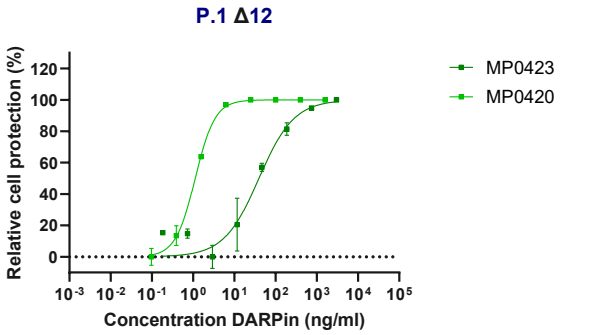
P.1 Δ12
Relative cell protection (%)
Concentration DARPin (ng/ml)
MP0423
MP0420

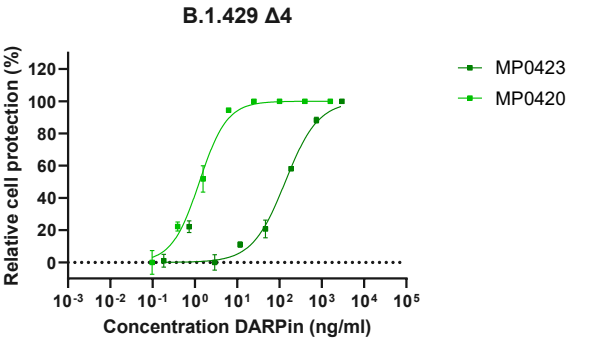
B.1.429 Δ4
Relative cell protection (%)
Concentration DARPin (ng/ml)
MP0423
MP0420

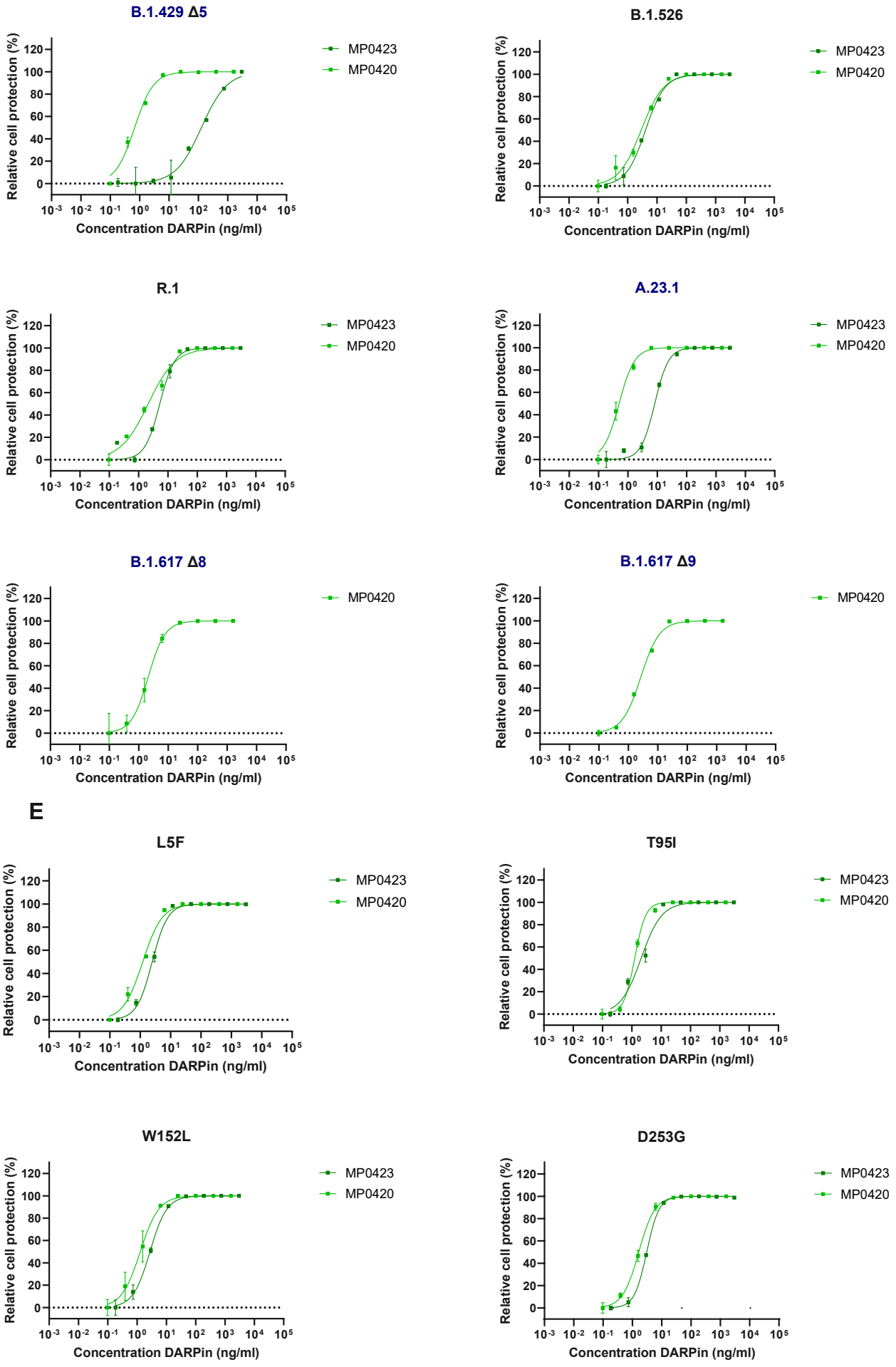
B.1.429 Δ5
B.1.526
R.1
A.23.1
B.1.617 Δ8
B.1.617 Δ9
E
L5F
T95I
W152L
D253G
MP0423
MP0420
Relative cell protection (%)
Concentration DARPin (ng/ml)

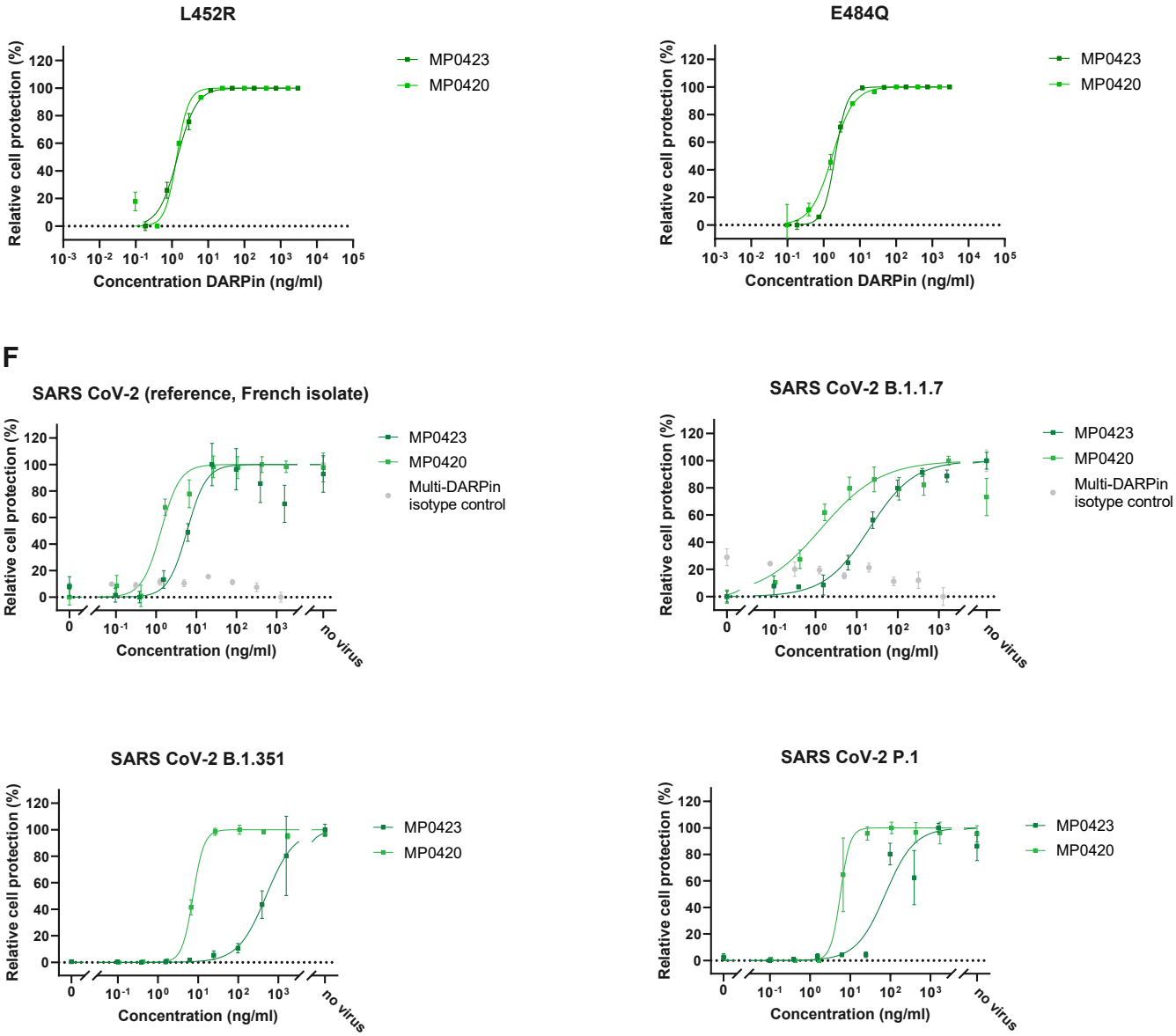

Supplementary Figure 3: Titration curves for ensovibep (MP0420) and its RBD-binding domains (i.e. RBD-1, RBD-2 and RBD-3), MP0423, REGN10933 and REGN10987 to determine IC_{50} neutralization potencies on multiple spike mutants and variants summarized in Table 1. Reported is the mean +/- SEM (standard error of the mean). **A)** VSV-based pseudovirus assay on variants carrying multiple spike mutations as specified in Table 1; **B)** VSV-based pseudovirus assay on single mutations present in different variants; **C)** VSV-based pseudovirus assay on single mutations present in high frequency, reported as resistance mutations for other therapeutics or located within the RBD epitope; **D)** Lentivirus-based pseudovirus assay on variants carrying multiple spike mutations as specifed in Table 1; **F)** Lentivirus-based pseudovirus assay on single mutations present in different variants, analyzed in a D614G background; **F)** SARS-CoV-2 neutralization assay on the globally most diffused variants B.1.1.7, B.1.351 and P.1 compared to wild type.

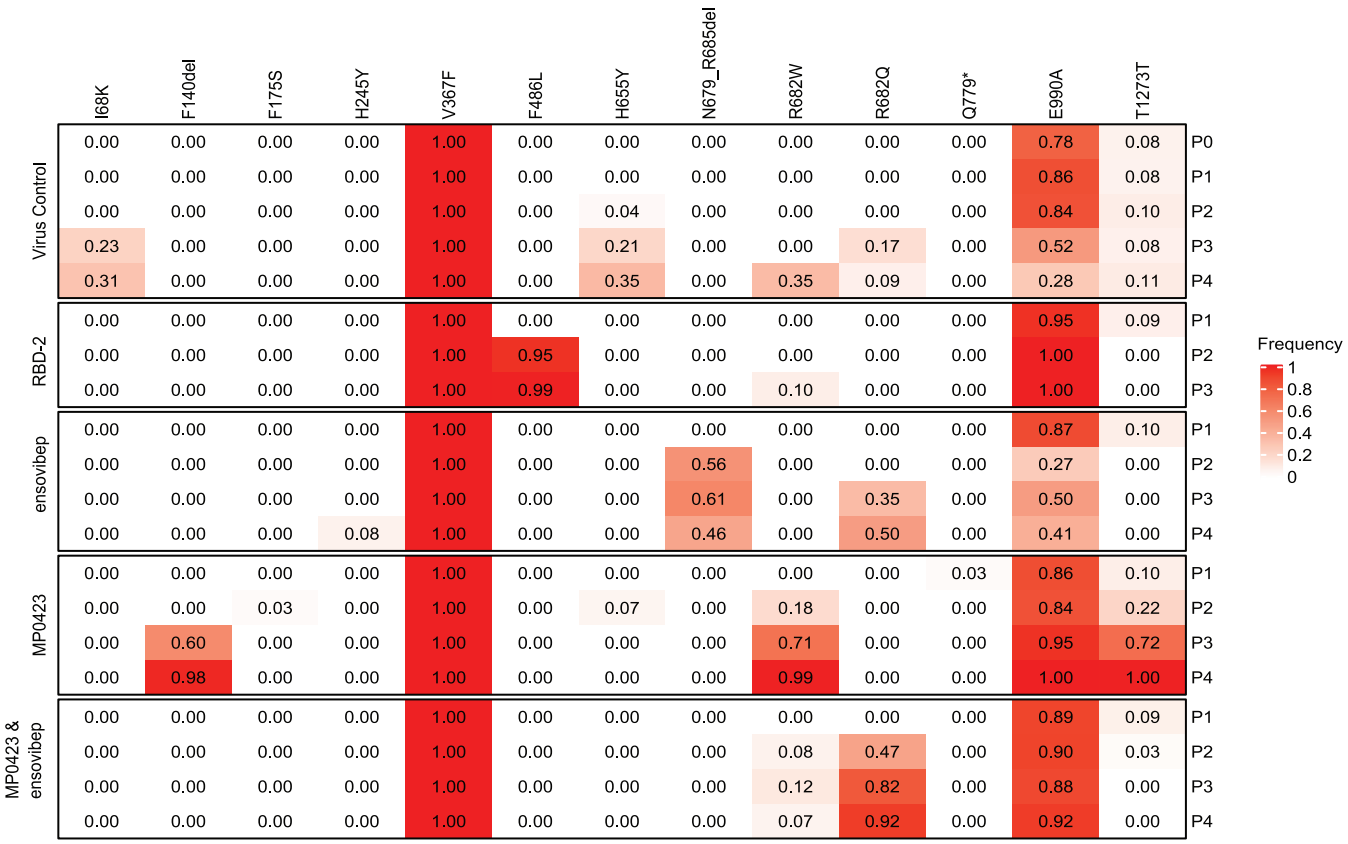

Supplementary Figure 4: Identification of escape mutations in viral passages using deep sequencing
SARS-CoV-2 virus was serially passaged with the mono-valent DARPin binder RBD-2, the multispecific DARPin® candidates ensovibep and MP0423 or a combination of both multispecific DARPin® candidates. To identify putative escape mutations in the spike protein, RNA was extracted and sequenced from supernatant of wells with the greatest selective pressure showing a significant cytopathic effect (see Figure 2 for the experimental design). All variants in the Spike protein relative to the reference genome (NC_045512.2) are shown. Passage 0 of the virus control corresponds to the inoculum used for all experiments. The color of the fields is proportional to the fraction of the reads containing the respective variant (red= 1.0 white=0.0).

References

1 Andreano, E. *et al.* SARS-CoV-2 escape in vitro from a highly neutralizing COVID-19 convalescent plasma. *bioRxiv*, doi:10.1101/2020.12.28.424451 (2020).

2 Voloch, C. M. *et al.* Novel circulating lineage of SARS-CoV-2 in the state of Rio de Janeiro Brazil originated from B.1.1.28 lineage. *medRxiv*, doi:10.1101/2020.12.23.20248598 (2020).

3 Thomson, E. C. *et al.* The circulating SARS-CoV-2 spike variant N439K maintains fitness while evading antibody-mediated immunity. *bioRxiv*, doi:10.1101/2020.11.04.355842 (2020).

4 Wang, P. *et al.* Increased Resistance of SARS-CoV-2 Variants B.1.351 and B.1.1.7 to Antibody Neutralization. *bioRxiv*, doi:10.1101/2021.01.25.428137 (2021).

5 Kupferschmidt, K. Fast-spreading U.K. virus variant raises alarms. *Science* **371**, 9-10, doi:10.1126/science.371.6524.9 (2021).

6 Tegally, H. *et al.* Emergence and rapid spread of a new severe acute respiratory syndrome-related coronavirus 2 (SARS-CoV-2) lineage with multiple spike mutations in South Africa. *medRxiv*, doi:10.1101/2020.12.21.20248640 (2020).

7 Zhou, D. *et al.* Evidence of escape of SARS-CoV-2 variant B.1.351 from natural and vaccine-induced sera. *Cell* **184**, 2348-2361 e2346, doi:10.1016/j.cell.2021.02.037 (2021).

8 Yi, C. *et al.* Key residues of the receptor binding motif in the spike protein of SARS-CoV-2 that interact with ACE2 and neutralizing antibodies. *Cell Mol Immunol* **17**, 621-630, doi:10.1038/s41423-020-0458-z (2020).

9 Wang, Z. *et al.* mRNA vaccine-elicited antibodies to SARS-CoV-2 and circulating variants. *bioRxiv*, doi:10.1101/2021.01.15.426911 (2021).

10 Liu, Z. *et al.* Identification of SARS-CoV-2 spike mutations that attenuate monoclonal and serum antibody neutralization. *Cell Host Microbe* **29**, 477-488 e474, doi:10.1016/j.chom.2021.01.014 (2021).

11 Garcia-Beltran, W. F. *et al.* Multiple SARS-CoV-2 variants escape neutralization by vaccine-induced humoral immunity. *Cell* **184**, 2523, doi:10.1016/j.cell.2021.04.006 (2021).

12 Mallapaty, S. COVID mink analysis shows mutations are not dangerous - yet. *Nature* **587**, 340-341, doi:10.1038/d41586-020-03218-z (2020).

13 Baum, A. *et al.* Antibody cocktail to SARS-CoV-2 spike protein prevents rapid mutational escape seen with individual antibodies. *Science* **369**, 1014-1018, doi:10.1126/science.abd0831 (2020).

14 Hodcroft, E. B. *et al.* Emergence and spread of a SARS-CoV-2 variant through Europe in the summer of 2020. *medRxiv*, doi:10.1101/2020.10.25.20219063 (2020).

15 Hou, Y. J. *et al.* SARS-CoV-2 D614G variant exhibits efficient replication ex vivo and transmission in vivo. *Science* **370**, 1464-1468, doi:10.1126/science.abe8499 (2020).

16 Choe, H. & Farzan, M. How SARS-CoV-2 first adapted in humans. *Science* **372**, 466-467, doi:10.1126/science.abi4711 (2021).

17 Ku, Z. *et al.* Molecular determinants and mechanism for antibody cocktail preventing SARS-CoV-2 escape. *Nat Commun* **12**, 469, doi:10.1038/s41467-020-20789-7 (2021).

18 Copin, R. *et al.* In vitro and in vivo preclinical studies predict REGEN-COV protection against emergence of viral escape in humans. *bioRxiv*, doi:10.1101/2021.03.10.434834v3 (2021).

536 19 Ledford, H. Antibody therapies could be a bridge to a coronavirus vaccine - but will the world
537 benefit? *Nature* **584**, 333-334, doi:10.1038/d41586-020-02360-y (2020).

538 20 Walser, M. *et al.* Highly potent anti-SARS-CoV-2 multivalent DARPin therapeutic candidates.
539 *bioRxiv*, doi:10.1101/2020.08.25.256339 (2020).

540 21 Cathcart, A. *et al.* The dual function monoclonal antibodies VIR-7831 and VIR-7832
541 demonstrate potent in vitro and in vivo activity against SARS-CoV-2. *bioRxiv*,
542 doi:10.1101/2021.03.09.434607v1 (2021).

543 22 Oude Munnink, B. B. *et al.* Transmission of SARS-CoV-2 on mink farms between humans and
544 mink and back to humans. *Science* **371**, 172-177, doi:10.1126/science.abe5901 (2021).

545 23 Yan, R. *et al.* Structural basis for the recognition of SARS-CoV-2 by full-length human ACE2.
546 *Science* **367**, 1444-1448, doi:10.1126/science.abb2762 (2020).

547 24 Callaway, E. Fast-spreading COVID variant can elude immune responses. *Nature* **589**, 500-501,
548 doi:10.1038/d41586-021-00121-z (2021).

549 25 Jones, B. E. *et al.* LY-CoV555, a rapidly isolated potent neutralizing antibody, provides
550 protection in a non-human primate model of SARS-CoV-2 infection. *bioRxiv*,
551 doi:10.1101/2020.09.30.318972 (2020).

552 26 Pinto, D. *et al.* Cross-neutralization of SARS-CoV-2 by a human monoclonal SARS-CoV
553 antibody. *Nature* **583**, 290-295, doi:10.1038/s41586-020-2349-y (2020).

554 27 Shi, R. *et al.* A human neutralizing antibody targets the receptor-binding site of SARS-CoV-2.
555 *Nature* **584**, 120-124, doi:10.1038/s41586-020-2381-y (2020).

556 28 Starr, T. N. *et al.* Deep Mutational Scanning of SARS-CoV-2 Receptor Binding Domain Reveals
557 Constraints on Folding and ACE2 Binding. *Cell* **182**, 1295-1310 e1220,
558 doi:10.1016/j.cell.2020.08.012 (2020).

559 29 Zahradnik, J. *et al.* SARS-CoV-2 RBD in vitro evolution follows contagious mutation spread, yet
560 generates an able infection inhibitor. *bioRxiv*, doi:10.1101/2021.01.06.425392v3 (2021).

561 30 Berger Rentsch, M. & Zimmer, G. A vesicular stomatitis virus replicon-based bioassay for the
562 rapid and sensitive determination of multi-species type I interferon. *PLoS One* **6**, e25858,
563 doi:10.1371/journal.pone.0025858 (2011).

564 31 Torriani, G. *et al.* Macropinocytosis contributes to hantavirus entry into human airway
565 epithelial cells. *Virology* **531**, 57-68, doi:10.1016/j.virol.2019.02.013 (2019).

566 32 Torriani, G. *et al.* Identification of Clotrimazole Derivatives as Specific Inhibitors of Arenavirus
567 Fusion. *J Virol* **93**, doi:10.1128/JVI.01744-18 (2019).

568 33 Matsuyama, S. *et al.* Enhanced isolation of SARS-CoV-2 by TMPRSS2-expressing cells. *Proc*
569 *Natl Acad Sci U S A* **117**, 7001-7003, doi:10.1073/pnas.2002589117 (2020).

570 34 Nao, N. *et al.* Consensus and variations in cell line specificity among human metapneumovirus
571 strains. *PLoS One* **14**, e0215822, doi:10.1371/journal.pone.0215822 (2019).

572 35 Neerukonda, S. N. *et al.* Establishment of a well-characterized SARS-CoV-2 lentiviral
573 pseudovirus neutralization assay using 293T cells with stable expression of ACE2 and
574 TMPRSS2. *PLoS One* **16**, e0248348, doi:10.1371/journal.pone.0248348 (2021).

575 36 Johnson, B. A. et al. Loss of furin cleavage site attenuates SARS-CoV-2 pathogenesis. Nature,
576 doi.org/10.1038/s41586-021-03237-4 (2021)

577 37 Lau, S.-Y. et al. Attenuated SARS-CoV-2 variants with deletions at the S1/S2 junction. EMI,
578 doi.org/10.1080/22221751.2020.1756700 (2020)

38. Li H, Handsaker B, Wysoker A, Fennell T, Ruan J, Homer N, Marth G, Abecasis G, Durbin R. 2009. The Sequence Alignment/Map format and SAMtools. Bioinformatics 25:2078–9.

39. Bolger AM, Lohse M, Usadel B. 2014. Trimmomatic: A flexible trimmer for Illumina sequence data. Bioinformatics 30:2114–2120.

40. Li H, Durbin R. 2009. Fast and accurate short read alignment with Burrows-Wheeler transform. Bioinformatics 25:1754–1760.

41. Wilm A, Aw PPK, Bertrand D, Yeo GHT, Ong SH, Wong CH, Khor CC, Petric R, Hibberd ML, Nagarajan N. 2012. LoFreq: A sequence-quality aware, ultra-sensitive variant caller for uncovering cell-population heterogeneity from high-throughput sequencing datasets. Nucleic Acids Res.

42. Cingolani P, Platts A, Wang LL, Coon M, Nguyen T, Wang L, Land SJ, Lu X, Ruden DM. 2012. A program for annotating and predicting the effects of single nucleotide polymorphisms, SnpEff: SNPs in the genome of Drosophila melanogaster strain w1118; iso-2; iso-3. Fly (Austin) 6:80–92.

43. R Core Team. 2018. R: A language and environment for statistical computing. R Foundation for Statistical Computing. R Foundation for Statistical Computing, Vienna, Austria. URL https://www.r-project.org/.

44. Gu Z, Eils R, Schlesner M. 2016. Complex heatmaps reveal patterns and correlations in multidimensional genomic data. Bioinformatics 32:2847–2849.